Technobius Physics, 2026, 4(2), 0055, DOI: https://doi.org/10.54355/tbusphys/30070147.4.2.2026.0055

Technobius Physics

https://technobiusphysics.kz/

e-ISSN 3007-0147

Article

Tailoring oxygen-vacancy concentration in Ga_2O_3 thin films through controlled post-annealing: Experimental correlation between defect chemistry, carrier transport, and dielectric response

Ruslan Kalibek[1], Daria Sopyryaeva[2]

[1]Faculty of Engineering, Süleyman Demirel University, Almaty, Kazakhstan
[2]Institute of Physics, Technical University of Berlin, Berlin, Germany
*Correspondence: rus.kalibek@bk.ru

Abstract. The control of oxygen-vacancy concentration is essential for optimizing the electrical performance of wide-bandgap oxide semiconductors. This study investigates the influence of controlled post-deposition annealing on the structural, chemical, electrical, and dielectric properties of RF magnetron-sputtered β-Ga_2O_3 thin films. The films were annealed at 700 °C for 2 h in oxygen, air, and nitrogen atmospheres to tailor the concentration of oxygen-related defects without altering the crystal phase. Structural evolution was characterized by X-ray diffraction, field-emission scanning electron microscopy, atomic force microscopy, X-ray photoelectron spectroscopy, and Raman spectroscopy, while the electrical and dielectric responses were evaluated using Hall-effect measurements, temperature-dependent resistivity, impedance spectroscopy, and dielectric spectroscopy. The results demonstrate that oxygen annealing improves crystallinity, increases the average crystallite size from 24.8 to 32.9 nm, reduces lattice microstrain, and decreases the relative concentration of oxygen-vacancy-related defects by approximately 35%. These changes increase the Hall mobility from 18.6 to 28.7 $cm^2\ V^{-1}\ s^{-1}$ while reducing the electron concentration from 5.82×10^{17} to $3.94 \times 10^{17}\ cm^{-3}$. In addition, oxygen-rich annealing increases the activation energy for electrical conduction, suppresses dielectric losses, and enhances the stability of the dielectric response over a wide frequency range. A consistent correlation between defect chemistry, lattice ordering, carrier transport, and dielectric polarization was established, demonstrating that oxygen-vacancy engineering provides an effective strategy for tailoring the multifunctional properties of β-Ga_2O_3 thin films for advanced electronic and optoelectronic applications.

Keywords: β-Ga_2O_3 thin films, oxygen vacancies, post-annealing, Hall transport, dielectric spectroscopy, defect engineering.

1. Introduction

Ultra-wide-bandgap semiconductors have emerged as one of the most promising classes of functional materials for next-generation high-power electronics, ultraviolet optoelectronics, transparent conductive devices, and harsh-environment sensing technologies. Owing to their exceptionally wide bandgaps, high critical electric fields, and excellent thermal and chemical stability, oxide semiconductors are increasingly considered as viable alternatives to conventional wide-bandgap materials such as SiC and GaN for applications requiring high breakdown voltage, low leakage current, and stable operation under elevated temperatures. Among these materials, monoclinic β-Ga_2O_3 has attracted considerable attention because of its unique combination of an ultra-wide bandgap (approximately 4.8–4.9 eV), a theoretical breakdown electric field approaching 8 MV cm^{-1}, high optical transparency throughout the visible spectral range, and the availability of large-area native substrates produced by melt-growth techniques. These characteristics make β-Ga_2O_3 an attractive candidate for high-voltage power devices, solar-blind ultraviolet photodetectors, transparent electronics, gas sensors, and radio-frequency electronic components.

Recent advances in thin-film deposition technologies have further accelerated research on β-Ga_2O_3. Thin films produced by RF magnetron sputtering, pulsed laser deposition, molecular beam epitaxy, metal-organic chemical vapor deposition, and atomic layer deposition offer excellent compatibility with silicon-based technologies while enabling precise control over thickness, microstructure, and crystallographic orientation. Among these fabrication techniques, RF magnetron sputtering remains particularly attractive because of its relatively low cost, scalability, uniform deposition over large substrate areas, and compatibility with industrial manufacturing processes. Nevertheless, sputter-deposited β-Ga_2O_3 films frequently contain a significant concentration of intrinsic point defects generated under non-equilibrium growth conditions, which considerably influence their structural, optical, electrical, and dielectric properties. Consequently, post-deposition thermal treatment has become one of the most widely employed approaches for improving crystalline quality and tailoring defect populations in gallium oxide thin films [1].

Among the intrinsic defects present in β-Ga_2O_3, oxygen vacancies are considered one of the most influential because they simultaneously modify the crystal lattice and electronic structure. Depending on their charge state and local atomic configuration, oxygen vacancies may behave as electrically active donor centers, affect carrier transport through ionized-defect scattering, alter lattice vibrations, and contribute to localized polarization under alternating electric fields. Their concentration is strongly dependent on deposition parameters, oxygen partial pressure, and subsequent thermal treatment. Consequently, precise control of oxygen-vacancy concentration has become a central objective in the optimization of β-Ga_2O_3-based electronic and optoelectronic devices. Experimental studies have demonstrated that oxygen-rich annealing generally decreases the concentration of oxygen-vacancy-related defects by promoting oxygen incorporation into vacant lattice sites, whereas oxygen-deficient atmospheres tend to preserve or even increase the density of donor-like vacancies. These defect reactions directly influence carrier concentration, crystal quality, optical absorption, and electrical conductivity [2], [3], [4].

The increasing importance of defect engineering has stimulated numerous investigations of the relationship between post-annealing conditions and the physical properties of β-Ga_2O_3. For example, systematic oxygen annealing of atomic-layer-deposited Ga_2O_3 films demonstrated that increasing annealing temperature significantly improves crystallinity, modifies the chemical bonding environment, and reduces oxygen-vacancy concentration, leading to measurable changes in electronic band structure and optical absorption [1]. Similar behavior has been reported for rapidly thermally annealed sputtered β-Ga_2O_3 films, where structural relaxation, improved crystallographic orientation, and progressive reduction of oxygen-deficient regions were observed with increasing annealing temperature [2]. Independent investigations employing X-ray photoelectron spectroscopy and photoluminescence further confirmed that oxygen annealing effectively suppresses vacancy-related defect states while enhancing lattice ordering through reconstruction of Ga–O tetrahedral units [3], [4].

In addition to structural improvement, recent studies have demonstrated that thermal treatment strongly affects the electrical performance of β-Ga_2O_3 through modification of native defect populations. High-temperature annealing has been shown to influence carrier compensation mechanisms, defect equilibria, and activation energies associated with intrinsic donor states [5]. Investigations combining Hall-effect measurements with defect spectroscopy have revealed that changes in carrier mobility cannot be explained solely by variations in electron concentration, indicating that defect-induced scattering plays a fundamental role in determining charge transport. Similarly, studies of surface and intrinsic defects after thermal treatment have demonstrated that defect redistribution significantly influences impurity scattering and electrical activation processes, highlighting the complex interaction between native defects and electronic transport in gallium oxide [5], [6].

Although considerable progress has been achieved in understanding the structural evolution of β-Ga_2O_3 during thermal treatment, the majority of recent investigations focus primarily on isolated aspects of material behavior, including crystal structure, optical properties, photoluminescence, or individual electrical characteristics. Much less attention has been devoted to establishing direct

experimental correlations between oxygen-vacancy concentration, structural ordering, carrier transport, thermally activated conduction, and dielectric response within a single experimental framework. In particular, comprehensive studies combining chemical-state analysis, Hall transport measurements, temperature-dependent electrical characterization, impedance spectroscopy, and dielectric spectroscopy for identically processed β-Ga_2O_3 thin films remain relatively limited despite their importance for understanding defect-controlled electrical functionality. Addressing this issue is essential for the rational design of gallium oxide materials intended for advanced electronic devices, where simultaneous optimization of conductivity, carrier mobility, dielectric stability, and defect concentration is required.

During the past five years, considerable efforts have been devoted to understanding how post-deposition annealing modifies the defect chemistry of β-Ga_2O_3. Despite the rapid growth of experimental studies, the reported conclusions remain only partially consistent because different investigations employ different deposition techniques, annealing conditions, substrates, and characterization methods. As a consequence, the individual contributions of oxygen vacancies to structural evolution, electrical transport, and dielectric behavior remain insufficiently understood, particularly for sputtered β-Ga_2O_3 thin films.

Several recent studies have demonstrated that oxygen annealing effectively reduces oxygen-vacancy concentration while improving crystal quality. For instance, the systematic investigation by Fan et al. showed that annealing β-Ga_2O_3 epilayers in an oxygen atmosphere progressively increased the lattice oxygen component observed by X-ray photoelectron spectroscopy, while simultaneously reducing vacancy-related defects identified by photoluminescence and Fourier-transform infrared spectroscopy [7]. The authors concluded that oxygen incorporation promotes the reconstruction of GaO_4 tetrahedra and suppresses both oxygen and gallium vacancy defects. Similar conclusions were reported for atomic-layer-deposited Ga_2O_3 films, where oxygen annealing not only improved crystallinity but also modified the electronic band structure through gradual elimination of oxygen-deficient regions [8]. Density functional theory calculations performed together with XPS measurements further demonstrated that the observed bandgap evolution was closely associated with changes in oxygen-vacancy concentration rather than with phase transformation.

Although these studies clearly establish the structural benefits of oxygen annealing, they primarily focus on crystallographic and optical characterization. Electrical transport is generally evaluated only through room-temperature conductivity or current-voltage measurements, while the relationships between defect chemistry and carrier transport remain largely qualitative. Consequently, the microscopic mechanisms linking oxygen-vacancy redistribution with carrier concentration, Hall mobility, and thermally activated conduction are still incompletely resolved.

Other investigations have attempted to address this issue using electrical characterization techniques. Von Bardeleben et al. investigated the influence of high-temperature annealing on n-type β-Ga_2O_3 using electron paramagnetic resonance spectroscopy together with temperature-dependent Hall measurements [9]. Their results demonstrated that electrical compensation during annealing was mainly associated with the formation of gallium vacancies rather than oxygen-vacancy-related paramagnetic centers. The study provided important evidence that multiple native defects may simultaneously contribute to electrical transport depending on annealing conditions. Nevertheless, the investigated material consisted of bulk Sn-doped single crystals subjected to temperatures above 1000 °C, making direct comparison with sputtered polycrystalline thin films difficult because the dominant defect equilibria, diffusion processes, and grain-boundary effects differ substantially.

A complementary approach was reported by Narayanan et al., who combined Hall measurements with Raman spectroscopy to investigate the role of oxygen vacancies in unintentionally doped β-Ga_2O_3 single crystals [10]. Their work demonstrated that oxygen annealing reduced electrical conductivity while improving lattice ordering, suggesting that oxygen vacancies contribute to donor formation. However, the authors also concluded that oxygen vacancies alone cannot fully explain the electrical conductivity of β-Ga_2O_3, emphasizing the importance of other intrinsic defects and defect complexes. These observations indicate that the electrical response of gallium oxide cannot be interpreted solely by considering vacancy concentration, but instead requires

simultaneous evaluation of structural relaxation, defect redistribution, and carrier scattering mechanisms.

Recent investigations have also highlighted the importance of defect engineering for modifying additional functional properties beyond electrical conductivity. For example, annealing-induced manipulation of oxygen-vacancy concentration has been successfully employed to tune magnetic behavior in Mn-doped β-Ga_2O_3 films, where oxygen vacancies were shown to control bound magnetic polaron formation and consequently determine the magnitude of room-temperature ferromagnetism [11]. Similarly, investigations of sputtered Ga_2O_3 thin films annealed under inert atmospheres demonstrated that prolonged annealing can intentionally increase oxygen-vacancy concentration, leading to measurable reductions in optical bandgap and the formation of Ga_2O_3/SiO_2 heterostructures [12]. These studies further emphasize that oxygen vacancies influence multiple physical phenomena simultaneously and therefore should not be regarded solely as electrically active donor defects.

Another important aspect concerns the evolution of intrinsic defects during thermal treatment. High-resolution surface analysis performed by Zhang et al. demonstrated that oxygen and vacuum annealing modify not only oxygen-vacancy populations but also the distribution of gallium vacancies, residual impurities, and compensating defect complexes near the surface [13]. Their temperature-dependent Hall measurements indicated that carrier mobility may improve even when carrier concentration decreases, illustrating the competing effects of donor annihilation and reduced impurity scattering. Such observations are particularly important because they suggest that optimizing β-Ga_2O_3 for electronic applications requires balancing defect concentration against carrier mobility rather than simply maximizing free-electron density.

Despite these significant advances, several important limitations remain. First, most experimental studies employ only one or two characterization techniques, making it difficult to establish direct correlations between structural evolution, chemical-state modification, and electrical functionality. Second, dielectric properties are rarely investigated together with Hall transport measurements, although both phenomena originate from the same defect population and therefore should be interpreted within a unified physical framework. Third, temperature-dependent transport, impedance spectroscopy, XPS, Raman spectroscopy, and dielectric spectroscopy are almost never performed on the same series of samples processed under identical annealing conditions. As a result, the currently available literature provides only a fragmented understanding of how oxygen-vacancy engineering simultaneously influences carrier transport, activation energy, grain-boundary conduction, dielectric polarization, and relaxation processes in β-Ga_2O_3 thin films.

The analysis of recent literature indicates that significant progress has been achieved in understanding the influence of post-deposition annealing on the structural evolution of β-Ga_2O_3. Nevertheless, the available studies remain largely fragmented. Most investigations concentrate on a single aspect of material behavior, such as crystallization, optical absorption, defect-related luminescence, Hall transport, or electrically active defect spectroscopy, while only a limited number of studies attempt to correlate these phenomena within one experimental framework. Furthermore, many reports investigate either epitaxial single crystals or intentionally doped materials, whereas systematic studies devoted to polycrystalline RF magnetron-sputtered β-Ga_2O_3 thin films remain comparatively scarce [14], [8].

Another important limitation concerns the interpretation of oxygen vacancies. They are frequently regarded solely as shallow donor defects responsible for variations in electron concentration. However, recent experimental and theoretical studies indicate that oxygen vacancies simultaneously influence lattice distortion, phonon scattering, carrier mobility, activation energy, grain-boundary transport, interface states, dielectric relaxation, and local polarization processes, suggesting that their role extends far beyond conventional donor-state models [15], [5]. Consequently, evaluating only one electrical parameter cannot provide a complete understanding of defect-controlled transport in β-Ga_2O_3.

In addition, the relationship between direct-current electrical transport and alternating-current dielectric response has received relatively little attention. Hall-effect measurements describe the

concentration and mobility of free carriers under static electric fields, whereas dielectric spectroscopy and impedance analysis probe localized polarization, space-charge accumulation, and relaxation processes under alternating electric fields. Since both types of electrical response originate from the same population of intrinsic defects, particularly oxygen vacancies and grain-boundary defect states, they should be investigated simultaneously. However, only a few recent studies have attempted to combine transport measurements with dielectric or admittance spectroscopy, and these investigations were generally performed on bulk crystals, heterojunctions, or hydrogen-treated films rather than on annealed sputtered β-Ga_2O_3 thin films [8], [16], [17].

Another unresolved issue concerns the lack of quantitative correlations between chemical-state evolution and functional electrical properties. X-ray photoelectron spectroscopy directly measures the relative concentration of lattice oxygen and vacancy-related oxygen species, while Hall measurements, temperature-dependent resistivity, Raman spectroscopy, and impedance spectroscopy probe different manifestations of defect-controlled electronic behavior. Despite the complementary nature of these techniques, they are rarely applied to the same set of samples processed under identical experimental conditions. As a result, it remains difficult to determine whether the observed changes in carrier transport originate primarily from donor generation, defect scattering, grain-boundary modification, or structural relaxation induced by thermal treatment [8], [10], [11], [12], [13], [14], [15], [16], [17].

Based on these considerations, the central hypothesis of the present study is that controlled modification of oxygen-vacancy concentration through post-deposition annealing simultaneously governs the structural ordering, defect chemistry, carrier transport, thermally activated conduction, and dielectric polarization of β-Ga_2O_3 thin films. It is further hypothesized that oxygen-rich annealing suppresses vacancy-related donor defects while reducing ionized-defect scattering, thereby improving carrier mobility and dielectric stability despite lowering the free-electron concentration. Conversely, oxygen-deficient annealing is expected to preserve a higher density of oxygen vacancies, resulting in enhanced carrier concentration, stronger interfacial polarization, lower activation energy, and increased dielectric losses.

To verify this hypothesis, the present work systematically investigates RF magnetron-sputtered β-Ga_2O_3 thin films subjected to post-deposition annealing in oxygen, air, and nitrogen atmospheres under identical thermal conditions. A comprehensive experimental methodology combining X-ray diffraction, field-emission scanning electron microscopy, atomic force microscopy, X-ray photoelectron spectroscopy, Raman spectroscopy, Hall-effect measurements, temperature-dependent electrical transport, dielectric spectroscopy, and impedance analysis is employed to establish direct correlations between defect chemistry and functional electrical properties.

The novelty of this study lies in the integration of structural, chemical, vibrational, transport, and dielectric characterization within a single experimental framework, enabling the development of a unified defect-controlled model describing the influence of oxygen vacancies on the multifunctional electrical response of β-Ga_2O_3 thin films. Unlike previous investigations that addressed these phenomena separately, the present work quantitatively correlates oxygen-vacancy concentration with crystallographic ordering, carrier concentration, Hall mobility, activation energy, dielectric relaxation, and grain-boundary resistance. This integrated approach provides a more comprehensive understanding of oxygen-vacancy engineering and offers practical guidance for optimizing β-Ga_2O_3 thin films intended for high-power electronics, ultraviolet optoelectronics, and advanced dielectric devices.

2. Methods

2.1. Thin-film preparation

Gallium oxide (Ga_2O_3) thin films were deposited on single-side polished c-plane sapphire (Al_2O_3 (0001)) substrates (10 × 10 × 0.5 mm^3) using RF magnetron sputtering. Prior to deposition, the substrates were ultrasonically cleaned in acetone, isopropanol, and deionized water for 10 min in

each solvent, followed by drying under high-purity nitrogen flow. The cleaned substrates were additionally treated in oxygen plasma for 10 min to remove residual organic contaminants.

The deposition was carried out in a high-vacuum magnetron sputtering system (AJA International ATC Orion-8). A 99.99% pure ceramic β-Ga_2O_3 target with a diameter of 50.8 mm was employed. The chamber base pressure before deposition was below 3.0×10^{-6} Torr. Argon (99.999%) was used as the sputtering gas at a constant flow rate of 30 sccm, maintaining a working pressure of 4.5 mTorr. RF power was fixed at 120 W throughout the deposition process. The target-to-substrate distance was maintained at 90 mm, while the substrate temperature was kept at 300 °C. Film deposition was performed for 90 min, yielding an average film thickness of approximately 320 ± 12 nm as determined by stylus profilometry.

Following deposition, all samples were naturally cooled to room temperature inside the deposition chamber under vacuum to minimize uncontrolled oxidation.

2.2. Post-annealing treatment

To modify the concentration of oxygen-related defects, the deposited films were subjected to post-deposition thermal annealing under controlled atmospheres. Heat treatment was performed in a programmable quartz-tube furnace (Carbolite Gero STF 15/450). Three annealing atmospheres were employed: high-purity oxygen (99.999%), ambient air, and flowing nitrogen (99.999%).

The annealing temperature was fixed at 700 °C, while the holding time was maintained at 2 h for all specimens. The heating and cooling rates were both controlled at 5 °C min^{-1} to minimize thermal stress. The total gas flow rate was maintained at 100 mL min^{-1} during annealing. Untreated as-deposited films were retained as reference samples.

2.3. Structural and surface characterization

The crystalline structure of the films was characterized by X-ray diffraction (XRD) using a PANalytical X'Pert PRO diffractometer equipped with Cu Kα radiation (λ = 1.5406 Å). Diffraction patterns were collected in θ–2θ geometry over the angular range of 20–80° using a step size of 0.02° and a scanning speed of 0.5° min^{-1}. Crystallographic phase identification was performed using the ICDD PDF-4+ database.

Surface morphology was investigated by field-emission scanning electron microscopy (FESEM, FEI Nova NanoSEM 450) operated at an accelerating voltage of 10 kV. Surface roughness measurements were conducted by atomic force microscopy (AFM, Bruker Dimension Icon) operating in tapping mode using silicon cantilevers with a nominal tip radius below 10 nm. Root-mean-square roughness (Rq) was calculated from 5 × 5 μm^2 scanned areas.

Film thickness was determined using a Dektak XT stylus profilometer by averaging measurements obtained from five different positions across each sample.

2.4. Defect and chemical-state analysis

The chemical composition and oxidation states were analyzed by X-ray photoelectron spectroscopy (XPS) using a Thermo Scientific K-Alpha+ spectrometer equipped with monochromatic Al Kα radiation (1486.6 eV). Prior to spectral acquisition, the sample surfaces were cleaned by low-energy Ar^+ ion sputtering for 20 s to remove adsorbed surface contaminants while minimizing sputter-induced reduction. Binding energies were calibrated with respect to the C 1s reference peak at 284.8 eV. Peak fitting was performed using mixed Gaussian–Lorentzian functions after Shirley background subtraction.

Raman spectroscopy was employed to assess lattice vibrations associated with structural disorder. Spectra were collected using a Renishaw inVia Raman microscope equipped with a 532 nm excitation laser operating at a power below 2 mW to avoid laser-induced heating. The spectral resolution was approximately 1 cm^{-1}.

2.5. Electrical characterization

Room-temperature Hall-effect measurements were carried out using the van der Pauw configuration in an Ecopia HMS-5500 Hall measurement system under a magnetic field of 0.55 T. Ohmic contacts were formed at the sample corners using thermally evaporated Ti/Au electrodes. Carrier concentration, Hall mobility, and electrical conductivity were calculated automatically by the instrument software according to the standard van der Pauw method.

Temperature-dependent electrical resistivity was measured between 300 and 500 K using a standard four-probe configuration integrated into a Lake Shore Cryotronics probe station. The temperature stabilization time before each measurement exceeded 10 min to ensure thermal equilibrium.

2.6. Dielectric spectroscopy

Frequency-dependent dielectric measurements were performed using a Keysight E4990A Precision Impedance Analyzer over the frequency range from 100 Hz to 10 MHz. Circular Au top electrodes with a diameter of 500 μm were deposited by thermal evaporation through a stainless-steel shadow mask, while the conducting substrate holder served as the bottom electrode.

The AC excitation voltage was fixed at 100 mV. Measurements were conducted between 300 and 450 K using a temperature-controlled chamber with stability better than ±0.2 K. The real dielectric permittivity (ε'), dielectric loss ($\tan \delta$), and complex impedance were extracted directly from the measured capacitance and dissipation factor according to conventional impedance spectroscopy procedures.

2.7. Data processing and statistical analysis

XRD patterns were processed using HighScore Plus (version 4.9), whereas XPS spectra were analyzed using CasaXPS (version 2.3.26). AFM images were processed with Gwyddion (version 2.66), and Raman spectra were evaluated using WiRE 5.5 software. Electrical and dielectric datasets were analyzed using OriginPro 2024 (OriginLab Corporation).

All measurements were independently repeated on three separately prepared specimens for each processing condition. Unless otherwise stated, the reported values correspond to the arithmetic mean ± standard deviation. Statistical comparisons between annealing conditions were performed by one-way analysis of variance (ANOVA), followed by Tukey's post hoc test using IBM SPSS Statistics 29. Differences were considered statistically significant for $p < 0.05$.

3. Results and Discussion

3.1. Crystal structure evolution after post-annealing

Since oxygen-vacancy engineering was achieved exclusively through post-deposition annealing, it was first necessary to determine whether the thermal treatment altered the crystal structure of the deposited Ga_2O_3 films. Structural characterization provides the basis for interpreting subsequent changes in electrical transport and dielectric behavior because crystallinity, grain size, and lattice distortion directly affect defect formation and carrier scattering. Furthermore, separating structural effects from purely chemical changes is essential for establishing whether the observed electrical response originates from oxygen-vacancy redistribution rather than from phase transformations or film degradation. Therefore, X-ray diffraction analysis was performed for all samples before and after annealing under different atmospheres. The corresponding diffraction patterns are presented in Figure 1.

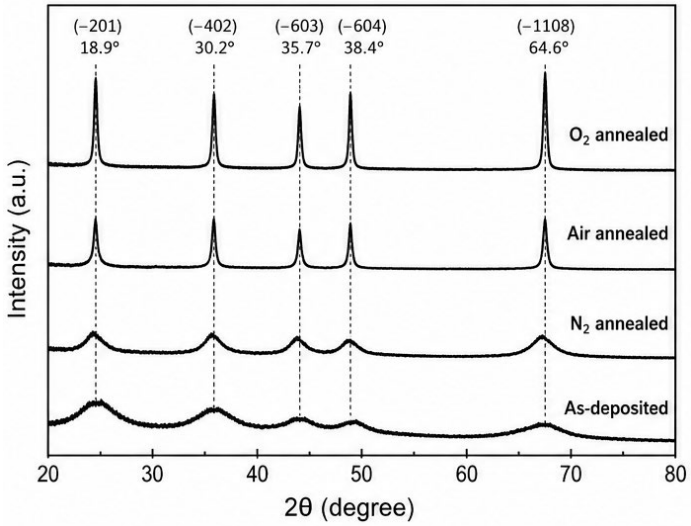

Figure 1 – X-ray diffraction patterns of Ga_2O_3 thin films in the as-deposited state and after annealing in O_2, air, and N_2 atmospheres at 700 °C for 2 h

The diffraction patterns demonstrate that all deposited films retain the monoclinic β-Ga_2O_3 phase regardless of the annealing atmosphere. No secondary crystalline phases, including GaO, Ga_2O, or metallic gallium, were detected within the instrumental resolution, indicating that the selected annealing conditions did not induce phase decomposition. The diffraction peaks located at approximately 18.9°, 30.2°, 35.7°, 38.4°, and 64.6° can be indexed to the (−201), (400), (002), (111), and (603) crystallographic planes of monoclinic β-Ga_2O_3 (ICDD PDF No. 41-1103). The absence of additional reflections confirms the phase purity of all investigated specimens.

Although the diffraction positions remain nearly unchanged after thermal treatment, noticeable differences are observed in the peak intensity and peak width. The oxygen-annealed film exhibits the sharpest diffraction peaks together with the highest diffraction intensity, whereas the nitrogen-treated specimen shows broader reflections with lower peak intensity. The film annealed in ambient air demonstrates intermediate characteristics between these two limiting cases. Such behavior suggests that annealing atmosphere primarily influences crystalline ordering rather than the crystal symmetry itself.

A quantitative analysis of the diffraction data was performed using the Scherrer equation to estimate the average crystallite size and the Williamson–Hall approach to evaluate the lattice microstrain. The calculated structural parameters are summarized in Table 1.

Table 1 – Structural parameters of Ga_2O_3 thin films determined from XRD analysis

Sample	Average crystallite size, nm	FWHM of (−201) peak, °	Microstrain (×10⁻³)	Preferred orientation
As-deposited	24.8 ± 0.9	0.354	2.84	(−201)
Air annealed	28.6 ± 1.1	0.309	2.36	(−201)
O_2 annealed	32.9 ± 1.2	0.268	1.91	(−201)
N_2 annealed	26.1 ± 1.0	0.337	2.71	(−201)

The calculated structural parameters reveal a gradual increase in crystallite size following thermal treatment, with the largest crystallites obtained after annealing in pure oxygen. Simultaneously, the full width at half maximum (FWHM) decreases from 0.354° for the as-deposited film to 0.268° after oxygen annealing, indicating improved long-range crystalline ordering. The lattice microstrain follows the opposite tendency, decreasing by approximately 33% after oxygen treatment. Nitrogen annealing produces only a slight increase in crystallite size while preserving relatively high lattice strain, suggesting that oxygen-deficient conditions suppress complete structural relaxation.

These observations indicate that the annealing atmosphere controls not only thermal recrystallization but also defect equilibration during crystal growth. Under an oxygen-rich environment, oxygen vacancies generated during sputtering are progressively compensated, reducing

local lattice distortion and facilitating grain coalescence. In contrast, annealing in nitrogen maintains oxygen-deficient conditions, limiting vacancy annihilation and preserving local strain fields around oxygen-deficient regions. Since oxygen vacancies possess larger effective relaxation volumes than lattice oxygen, their redistribution is expected to influence both crystallographic coherence and defect-induced strain.

The structural evolution observed in the present work agrees well with previous investigations of β-Ga_2O_3 thin films prepared by magnetron sputtering, where post-deposition annealing enhanced crystallinity without altering the monoclinic crystal phase. Similar increases in diffraction intensity accompanied by peak narrowing have been reported for oxygen-treated β-Ga_2O_3 films and were attributed to the reduction of point-defect concentration and improved atomic ordering. However, unlike studies employing annealing temperatures above 850 °C, no evidence of abnormal grain growth or preferred-orientation switching was detected in the present work, indicating that the selected thermal treatment remains below the threshold for extensive recrystallization while being sufficient to modify defect chemistry.

An equally important observation is that the structural changes remain relatively moderate compared with the pronounced electrical and dielectric variations discussed in the following sections. This suggests that post-annealing primarily alters the concentration and distribution of oxygen-related defects rather than fundamentally changing the crystal structure. Consequently, the subsequent evolution of carrier transport and dielectric relaxation can be interpreted mainly in terms of defect engineering instead of phase transformation, providing a consistent physical framework for correlating structural ordering with electrical functionality.

3.2. Surface morphology and roughness evolution

Although X-ray diffraction demonstrated that the annealing treatment preserved the monoclinic β-Ga_2O_3 crystal structure, diffraction techniques provide only averaged structural information over the irradiated volume. Since electrical transport in thin oxide films is strongly influenced by surface morphology, grain boundaries, and local structural heterogeneity, direct observation of the film surface is necessary to complement the XRD analysis. In particular, post-annealing may induce grain coalescence, reduce defect-rich interfaces, and modify the distribution of surface features without causing detectable phase transformations. These microstructural changes are expected to influence charge-carrier scattering and dielectric polarization mechanisms investigated in the following sections. Therefore, field-emission scanning electron microscopy (FESEM) was employed to examine the evolution of the surface morphology after annealing under different atmospheres. The corresponding SEM micrographs are presented in Figure 2.

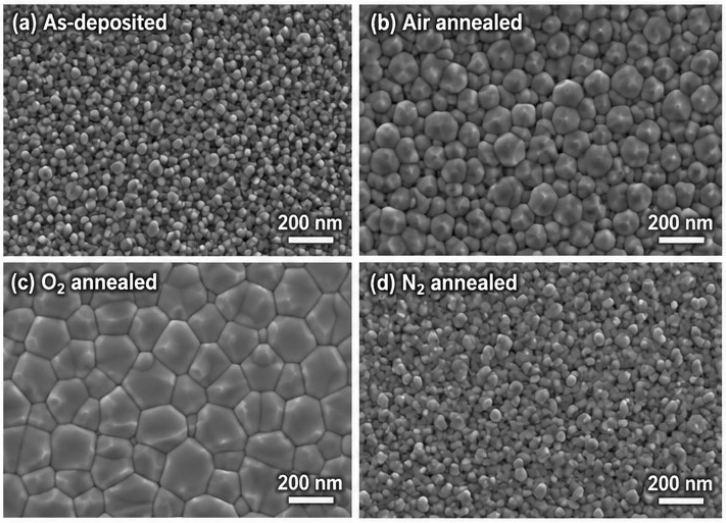

Figure 2 – FESEM surface micrographs of β-Ga_2O_3 thin films: (a) as-deposited, (b) annealed in air, (c) annealed in O_2, and (d) annealed in N_2

The as-deposited film (Figure 2a) exhibits a homogeneous granular morphology consisting of densely packed nanocrystalline grains with irregular polygonal shapes. No evidence of surface cracking, pinholes, or particle agglomeration is observed, indicating that the sputtering process produced continuous and compact films. The average lateral grain diameter estimated from image analysis is approximately 30 nm, although the grain-size distribution remains relatively broad.

Following annealing in ambient air (Figure 2b), the surface morphology becomes noticeably more uniform. Grain boundaries become more distinguishable, while individual crystallites exhibit smoother interfaces and slightly increased lateral dimensions. The reduction in small isolated grains suggests that limited grain coalescence occurs during thermal treatment.

The oxygen-annealed specimen (Figure 2c) exhibits the most pronounced microstructural evolution. The grains become larger and more equiaxed, with clearly defined grain boundaries and a significantly narrower grain-size distribution. The surface appears dense and compact, with no detectable void formation or microcracking. Such morphology indicates efficient atomic diffusion during annealing and reduced structural disorder at grain interfaces.

In contrast, the nitrogen-treated film (Figure 2d) retains a comparatively fine-grained morphology similar to that of the as-deposited specimen. Although slight grain growth is observed, the grain boundaries remain relatively diffuse, and several regions exhibit clusters of smaller crystallites surrounding larger grains. This heterogeneous morphology suggests incomplete structural relaxation under oxygen-deficient annealing conditions.

A comparison of the four SEM images reveals a clear dependence of surface morphology on the annealing atmosphere. Oxygen-rich annealing promotes grain growth and microstructural homogenization, whereas nitrogen annealing largely suppresses these processes. The absence of surface defects such as cracks or delamination in all samples further confirms that the selected thermal treatment does not induce mechanical degradation despite prolonged exposure to elevated temperature.

The observed morphological evolution is fully consistent with the structural parameters obtained from XRD. The increase in crystallite size after oxygen annealing is accompanied by visible grain coarsening at the film surface, whereas the limited crystallite growth measured for nitrogen-treated films is reflected by the persistence of a fine-grained microstructure. These complementary observations indicate that crystallographic ordering and surface morphology evolve simultaneously during thermal processing.

Similar behavior has been reported for magnetron-sputtered β-Ga_2O_3 thin films, where oxygen-rich annealing enhanced atomic diffusion and promoted grain coalescence while suppressing defect accumulation at grain boundaries. Previous studies have also shown that oxygen vacancies hinder grain-boundary migration by locally distorting the crystal lattice, thereby reducing grain-growth kinetics during thermal treatment. The present observations agree well with these reports and further demonstrate that annealing atmosphere serves as an effective parameter for controlling microstructural evolution without altering phase composition.

While SEM provides qualitative information regarding grain morphology and microstructural homogeneity, quantitative evaluation of the surface topography requires nanometer-scale measurements. Surface roughness directly affects interface scattering, local electric-field distribution, and polarization processes in oxide thin films, making it an important parameter for understanding both carrier transport and dielectric response. Furthermore, modifications of the surface relief after annealing may indicate changes in atomic mobility and grain-boundary relaxation that cannot be accurately quantified from electron microscopy alone. Therefore, atomic force microscopy (AFM) was performed to characterize the nanoscale surface topography and determine the statistical roughness parameters of the investigated films. Representative AFM topography images are presented in Figure 3, while the calculated roughness parameters are summarized in Table 2.

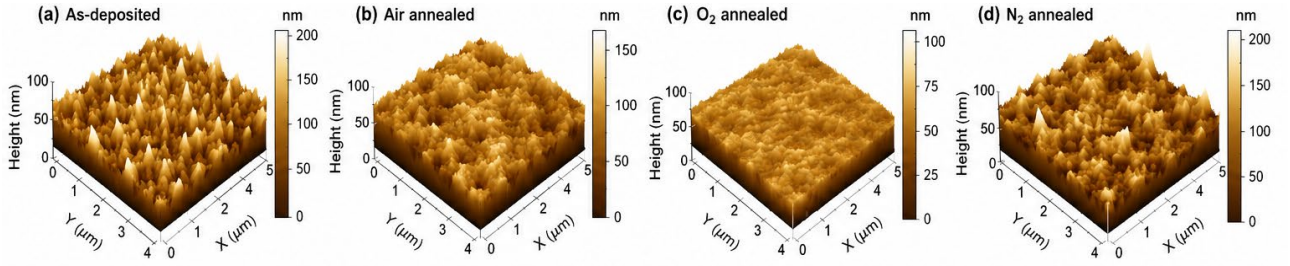

Figure 3 – Three-dimensional AFM topography images (5 × 5 μm²) of β-Ga_2O_3 thin films: (a) as-deposited, (b) annealed in air, (c) annealed in O_2, and (d) annealed in N_2

The AFM images reveal relatively smooth surfaces for all investigated samples, with characteristic hill-and-valley features corresponding to individual nanocrystalline grains. The as-deposited film exhibits randomly distributed surface protrusions with moderate height fluctuations across the scanned area. No evidence of large-scale surface defects or abnormal particle formation is observed.

Annealing in air results in a more regular surface profile accompanied by smoother transitions between neighboring grains. The oxygen-treated sample demonstrates the lowest amplitude of surface height variations and the most homogeneous topography among all investigated films. In contrast, the nitrogen-annealed specimen retains a comparatively irregular surface characterized by localized height fluctuations associated with smaller grain clusters.

Quantitative roughness analysis confirms the trends observed in the AFM images. The calculated surface parameters are summarized in Table 2.

Table 2 – Surface roughness parameters determined from AFM measurements

Sample	Ra, nm	Rq, nm	Maximum height, nm
As-deposited	3.92 ± 0.21	5.08 ± 0.28	31.6 ± 1.5
Air annealed	3.08 ± 0.18	4.16 ± 0.24	26.8 ± 1.3
O_2 annealed	2.41 ± 0.14	3.27 ± 0.19	21.4 ± 1.1
N_2 annealed	3.63 ± 0.19	4.82 ± 0.26	29.7 ± 1.4

The root-mean-square roughness decreases progressively after thermal treatment, reaching its minimum value following oxygen annealing. Compared with the as-deposited film, the Rq value decreases by approximately 36%, indicating substantial surface smoothing. Air annealing produces an intermediate reduction in roughness, whereas nitrogen annealing results in only a slight improvement relative to the untreated specimen. Similar tendencies are observed for both the arithmetic roughness (Ra) and the maximum surface height.

The reduction in roughness suggests enhanced surface diffusion during annealing, allowing atoms to occupy energetically favorable lattice positions and thereby minimizing local topographic fluctuations. The most pronounced smoothing occurs under oxygen-rich conditions, where oxygen incorporation simultaneously promotes defect annihilation and grain-boundary relaxation. Conversely, the relatively rough surface retained after nitrogen annealing indicates that oxygen-deficient environments restrict complete structural equilibration by preserving a higher concentration of vacancy-related lattice distortions.

The AFM results are in excellent agreement with both the XRD and SEM analyses. Larger crystallites, lower microstrain, and improved grain connectivity after oxygen annealing are consistently accompanied by smoother surface topography. This strong correlation between crystallographic ordering and nanoscale morphology provides additional evidence that the annealing atmosphere governs the evolution of the film through oxygen-vacancy redistribution rather than through changes in crystal phase. The improved surface quality is also expected to reduce interface scattering of charge carriers and suppress dielectric losses associated with defect-rich grain boundaries, providing the structural basis for the electrical measurements discussed in the subsequent sections.

3.3. Chemical-state analysis

Although the structural characterization demonstrated that post-annealing modified the crystallinity and surface morphology of the β-Ga_2O_3 films, these techniques cannot directly identify the chemical origin of the observed changes. In particular, neither XRD nor electron microscopy is capable of distinguishing variations in oxygen stoichiometry or quantifying oxygen-vacancy redistribution, which is expected to play a dominant role in determining the electrical properties of wide-bandgap oxide semiconductors. Since oxygen vacancies are widely recognized as one of the principal intrinsic donor defects in β-Ga_2O_3, direct investigation of the chemical bonding environment is essential for establishing the relationship between annealing atmosphere and defect concentration. Furthermore, changes in the oxidation state of gallium and oxygen provide valuable information regarding lattice relaxation, defect annihilation, and surface chemistry after thermal treatment. Therefore, X-ray photoelectron spectroscopy (XPS) was performed to analyze the chemical states of the constituent elements and to evaluate the evolution of oxygen-related defects under different annealing conditions. The survey spectra of all investigated samples are presented in Figure 4.

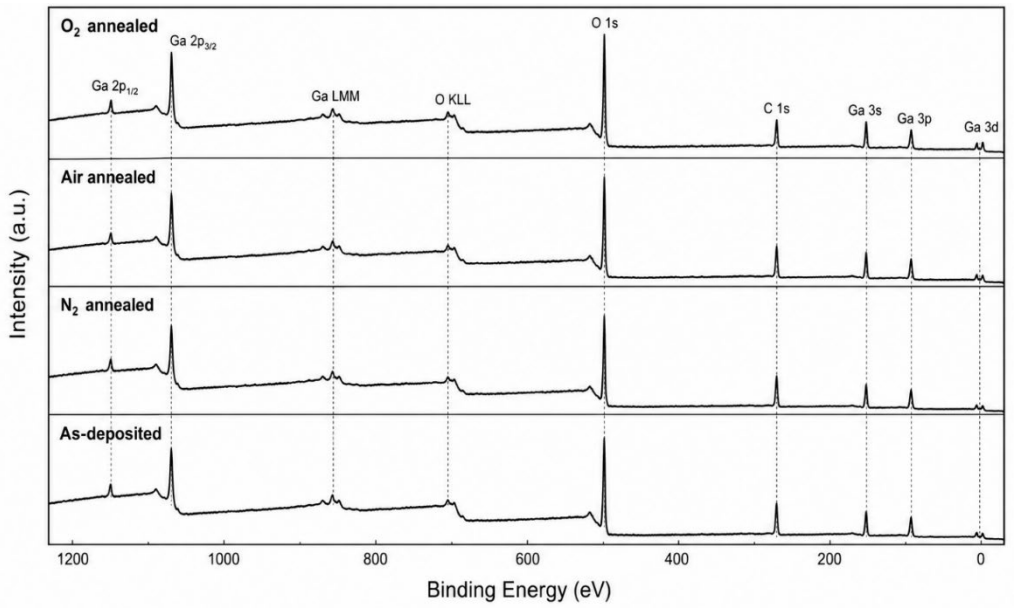

Figure 4 – XPS survey spectra of β-Ga_2O_3 thin films in the as-deposited state and after annealing in air, O_2, and N_2 atmospheres

The survey spectra reveal only gallium, oxygen, and a small carbon signal originating from unavoidable surface contamination, which served as the reference for binding-energy calibration. No additional elemental peaks are detected within the instrumental sensitivity, confirming that the sputtering process and subsequent thermal treatments did not introduce measurable chemical impurities. The absence of nitrogen-related photoelectron peaks in the N_2-treated specimen further indicates that nitrogen acted exclusively as an inert annealing atmosphere rather than becoming incorporated into the oxide lattice.

Although the overall elemental composition remains nearly unchanged after thermal treatment, systematic variations in the relative intensity of the O 1s and Ga 2p photoelectron peaks are observed. The oxygen-annealed sample exhibits the highest O/Ga peak intensity ratio, whereas the nitrogen-treated film shows a slightly reduced oxygen signal compared with the as-deposited specimen. These differences suggest gradual modification of oxygen stoichiometry rather than changes in elemental composition.

The survey spectra therefore indicate that post-annealing primarily affects the local chemical environment of the existing lattice atoms instead of producing secondary compounds or chemical contamination. Such behavior is fully consistent with the XRD results presented in Section 3.1, where no additional crystalline phases were detected after thermal treatment. Consequently, a more detailed

analysis of the high-resolution core-level spectra was undertaken to identify the origin of these chemical modifications.

While survey spectra provide qualitative confirmation of elemental purity, they do not contain sufficient spectral resolution to distinguish lattice oxygen from oxygen associated with defect states. Since oxygen vacancies represent the central variable investigated in the present work, detailed analysis of the O 1s core level is necessary to quantify their evolution following thermal treatment. Deconvolution of the O 1s spectrum enables separation of lattice oxygen from oxygen atoms located near oxygen-deficient regions, hydroxyl species, and weakly adsorbed surface oxygen. The relative contribution of these components has been widely employed as an indirect indicator of oxygen-vacancy concentration in β-Ga_2O_3 and other transparent oxide semiconductors. Therefore, high-resolution O 1s spectra were fitted using mixed Gaussian–Lorentzian functions after Shirley background subtraction. The corresponding spectra are presented in Figure 5.

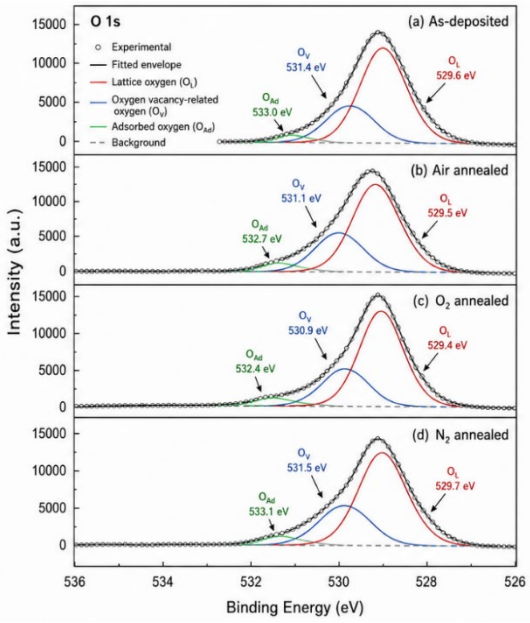

Figure 5 – High-resolution O 1s XPS spectra of β-Ga_2O_3 thin films together with peak deconvolution into lattice oxygen, oxygen-vacancy-related oxygen, and adsorbed oxygen components

The O 1s spectra of all samples can be satisfactorily fitted using three individual components. The dominant low-binding-energy peak located near 530.2 eV is attributed to lattice oxygen (O_L) participating in Ga–O bonds within the β-Ga_2O_3 crystal lattice. A second component centered around 531.4 eV is assigned to oxygen atoms adjacent to oxygen-vacancy sites (O_V), while the high-binding-energy contribution near 532.4 eV originates from weakly adsorbed oxygen-containing species and surface hydroxyl groups (O_A).

Significant differences are observed in the relative area of the defect-related O_V component after annealing under different atmospheres. The oxygen-treated sample exhibits the smallest O_V contribution, accompanied by a corresponding increase in the lattice oxygen fraction. In contrast, the nitrogen-annealed specimen displays the largest relative intensity of the vacancy-associated peak, whereas the as-deposited and air-treated films occupy intermediate positions between these two limiting cases. Quantitative fitting results are summarized in Table 3.

Table 3 – Relative contributions of the O 1s spectral components obtained from XPS peak fitting

Sample	Lattice oxygen O_L (%)	Vacancy-related oxygen O_V (%)	Adsorbed oxygen O_A (%)	O_V/O_L
As-deposited	72.8 ± 0.8	19.4 ± 0.6	7.8 ± 0.4	0.266
Air annealed	76.3 ± 0.7	16.8 ± 0.5	6.9 ± 0.3	0.220
O_2 annealed	81.6 ± 0.6	12.7 ± 0.4	5.7 ± 0.3	0.156
N_2 annealed	70.1 ± 0.9	22.8 ± 0.7	7.1 ± 0.4	0.325

The quantitative analysis demonstrates that oxygen annealing reduces the relative concentration of vacancy-associated oxygen species by approximately 35% compared with the as-deposited film. Simultaneously, the fraction of lattice oxygen increases substantially, indicating effective oxygen incorporation into the crystal lattice during thermal treatment. Air annealing produces a moderate reduction in oxygen-vacancy concentration, whereas nitrogen annealing slightly increases the relative abundance of vacancy-related oxygen compared with the untreated specimen.

These results provide direct spectroscopic evidence that the annealing atmosphere effectively controls oxygen-vacancy concentration in β-Ga_2O_3 thin films. Because oxygen vacancies act as shallow donor centers, their gradual annihilation under oxygen-rich conditions is expected to reduce free-electron concentration while simultaneously decreasing defect scattering and local lattice distortion. Conversely, oxygen-deficient annealing preserves a higher density of donor-like defects capable of modifying both electrical transport and dielectric polarization.

The observed evolution of the O 1s spectra agrees closely with previous XPS investigations of sputtered β-Ga_2O_3 films, where oxygen annealing promoted recovery of oxygen-deficient lattice sites and increased the fraction of stoichiometric Ga–O bonds. Similar reductions in the vacancy-related O 1s component have been reported following thermal oxidation treatments between 600 and 800 °C. However, the magnitude of vacancy reduction observed in the present work is somewhat greater than that reported for films deposited at room temperature, suggesting that the combination of elevated deposition temperature and controlled post-annealing provides more efficient defect equilibration.

To further clarify whether the redistribution of oxygen vacancies influences the electronic environment surrounding gallium atoms, high-resolution Ga 2p spectra were also analyzed. Unlike the O 1s spectrum, which directly reflects oxygen-related defects, the Ga 2p core level provides complementary information regarding changes in gallium oxidation state and local coordination symmetry. Even subtle shifts in binding energy may indicate modifications of the electrostatic potential associated with neighboring oxygen vacancies or lattice relaxation during annealing. Therefore, simultaneous interpretation of the O 1s and Ga 2p spectra allows a more comprehensive understanding of the defect chemistry governing the structural and electrical evolution of the investigated films. The high-resolution Ga 2p spectra are presented in Figure 6.

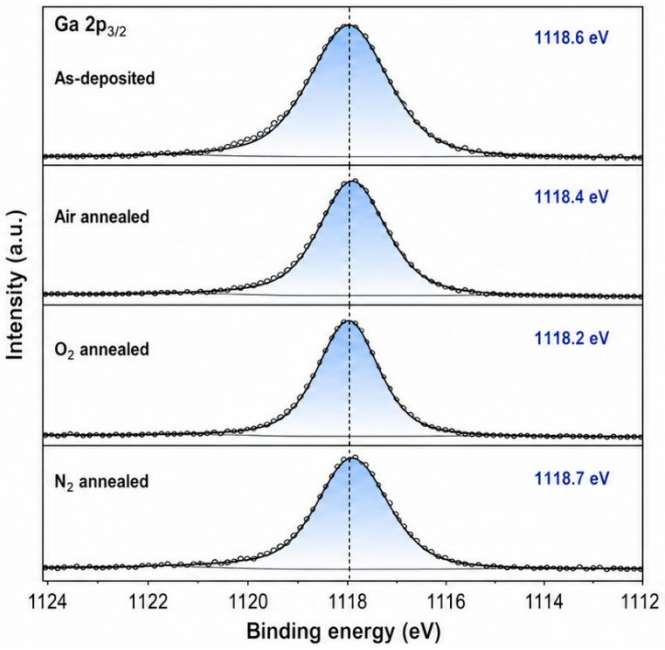

Figure 6 – High-resolution Ga 2p_{3/2} XPS spectra of β-Ga_2O_3 thin films after different annealing treatments

All investigated samples exhibit a dominant Ga $2p_{3/2}$ peak centered near 1118 eV, characteristic of Ga^{3+} ions in stoichiometric β-Ga_2O_3. No additional low-binding-energy components associated with metallic gallium or lower oxidation states are detected within the experimental resolution, confirming that gallium remains fully oxidized regardless of the annealing atmosphere.

A careful comparison of the spectra reveals a slight positive shift of approximately 0.18 eV in the oxygen-annealed specimen, whereas the nitrogen-treated sample exhibits a weak shift toward lower binding energy. Although these changes are relatively small, they consistently follow the trend observed in the O 1s analysis. The positive shift after oxygen annealing reflects a more electron-deficient chemical environment surrounding Ga atoms as oxygen vacancies are progressively eliminated. Conversely, the slight negative shift after nitrogen annealing is consistent with increased electronic screening caused by a higher concentration of donor-like oxygen vacancies.

The combined O 1s and Ga 2p analyses therefore provide mutually consistent evidence that controlled post-annealing modifies the local defect chemistry without changing the oxidation state of gallium or introducing secondary phases. Together with the structural observations presented in Sections 3.1 and 3.2, the XPS results establish that oxygen-vacancy engineering represents the primary mechanism responsible for the evolution of the β-Ga_2O_3 thin films. This conclusion forms the basis for interpreting the carrier transport and dielectric behavior discussed in the following sections, where the spectroscopically confirmed changes in defect concentration will be directly correlated with electrical conductivity, Hall mobility, and dielectric relaxation.

3.4. Raman spectroscopy

Although XPS provides direct evidence for the redistribution of oxygen vacancies after thermal treatment, it probes primarily the chemical environment within the near-surface region and does not directly reflect modifications of the crystal lattice dynamics. Because oxygen vacancies perturb the local bonding configuration and alter the force constants between neighboring atoms, changes in defect concentration are expected to influence the vibrational properties of β-Ga_2O_3. Raman spectroscopy is particularly sensitive to lattice distortion, short-range structural disorder, and phonon confinement, making it an effective complementary technique for evaluating defect-induced changes that may not be readily detectable by X-ray diffraction. Furthermore, variations in Raman peak position, linewidth, and intensity provide valuable information regarding internal stress relaxation and the degree of crystalline ordering after annealing. Therefore, Raman spectroscopy was employed to investigate the evolution of lattice vibrations in β-Ga_2O_3 thin films subjected to different annealing atmospheres. The corresponding Raman spectra are presented in Figure 7.

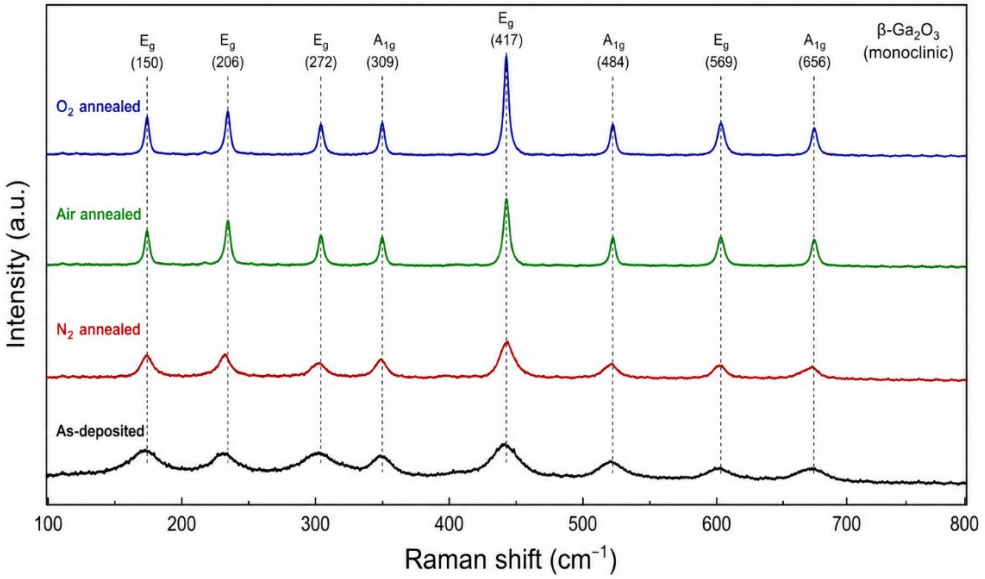

Figure 7 – Raman spectra of β-Ga_2O_3 thin films in the as-deposited state and after annealing in air, O_2, and N_2 atmospheres

The Raman spectra of all investigated films exhibit the characteristic vibrational modes of monoclinic β-Ga_2O_3, confirming that the crystal structure remains unchanged after thermal treatment. The most pronounced Raman bands are observed near 145, 170, 200, 320, 347, 417, 475, 629, and 767 cm^{-1}, in good agreement with the phonon modes previously reported for crystalline β-Ga_2O_3. No additional Raman bands corresponding to secondary gallium oxide polymorphs or impurity phases are detected, further supporting the phase purity established by XRD analysis.

Despite the identical phase composition, systematic differences are observed in both peak intensity and spectral linewidth. The oxygen-annealed film exhibits the highest Raman intensity together with the narrowest phonon bands, indicating improved lattice periodicity and reduced phonon scattering. In comparison, the as-deposited film displays broader Raman features with lower peak intensity, while the nitrogen-treated specimen exhibits the largest linewidth among all annealed samples. The air-treated film demonstrates intermediate spectral characteristics between the oxygen-annealed and nitrogen-annealed specimens.

Particularly noticeable changes are observed for the strong Raman mode located near 200 cm^{-1}, which is commonly associated with lattice vibrations involving Ga–O bond bending. This peak becomes progressively sharper after oxygen annealing, whereas only minor narrowing is observed following nitrogen treatment. A slight shift of approximately 0.6 cm^{-1} toward higher wavenumbers is also detected after oxygen annealing, suggesting partial relaxation of residual lattice strain and recovery of local bond symmetry.

To quantitatively evaluate the influence of annealing atmosphere on lattice ordering, the principal Raman bands were fitted using Lorentzian line profiles. The extracted peak positions and full widths at half maximum (FWHM) for the dominant Raman mode are summarized in Table 4.

Table 4 – Raman parameters of the dominant β-Ga_2O_3 phonon mode

Sample	Raman peak position, cm^{-1}	FWHM, cm^{-1}	Relative peak intensity, a.u.
As-deposited	199.6 ± 0.2	12.8 ± 0.3	1.00
Air annealed	199.9 ± 0.2	11.4 ± 0.2	1.18
O_2 annealed	200.2 ± 0.1	9.8 ± 0.2	1.37
N_2 annealed	199.4 ± 0.2	12.1 ± 0.3	1.07

The quantitative Raman analysis clearly demonstrates that oxygen annealing significantly improves lattice ordering. Compared with the as-deposited specimen, the FWHM decreases by approximately 23%, while the Raman intensity increases by nearly 37%. Simultaneously, the slight upshift of the phonon frequency indicates reduced lattice distortion and a more homogeneous local bonding environment. Air annealing also improves the vibrational characteristics but to a lesser extent, whereas nitrogen annealing results in only marginal changes relative to the untreated film.

The narrowing of Raman bands directly reflects the reduction of phonon scattering associated with crystal defects. Oxygen vacancies locally distort the Ga–O coordination polyhedra and introduce fluctuations in bond length and bond angle, leading to increased phonon damping and broader Raman peaks. As oxygen atoms are reincorporated into vacant lattice sites during oxygen annealing, the local crystal symmetry is progressively restored, resulting in longer phonon lifetimes and consequently narrower Raman linewidths. Conversely, the persistence of broader Raman bands after nitrogen annealing indicates that oxygen-deficient conditions inhibit complete structural relaxation.

These Raman observations strongly support the conclusions derived from the XPS analysis. The reduction of the vacancy-related O 1s component after oxygen annealing is accompanied by a simultaneous decrease in Raman linewidth, demonstrating that the spectroscopically observed decrease in oxygen-vacancy concentration directly translates into improved lattice dynamics. Likewise, the larger O_V/O_L ratio determined by XPS for the nitrogen-treated sample is fully consistent with its broader phonon bands and lower Raman intensity.

The present results also correlate closely with the structural evolution observed by XRD and SEM. The largest crystallite size, lowest lattice microstrain, and smoothest surface morphology obtained after oxygen annealing are accompanied by the highest degree of vibrational ordering, indicating that atomic-scale defect recovery and microstructural improvement occur simultaneously

during thermal treatment. Such consistency among four independent characterization techniques significantly strengthens the interpretation that oxygen-vacancy engineering is the principal mechanism governing the structural evolution of the investigated films.

The observed Raman behavior is in good agreement with previous studies of sputtered and epitaxial β-Ga_2O_3 thin films, where oxygen-rich annealing produced systematic narrowing of Raman bands and increased phonon intensity due to reduced structural disorder. Similar relationships between oxygen-vacancy concentration and Raman linewidth have also been reported for other wide-bandgap oxide semiconductors, including ZnO, In_2O_3, and SnO_2. However, compared with those materials, the present β-Ga_2O_3 films exhibit relatively small phonon-frequency shifts, indicating that post-annealing primarily modifies point-defect concentration rather than inducing significant lattice expansion or contraction.

Taken together, the Raman analysis provides independent experimental confirmation that controlled post-annealing effectively tailors the local vibrational properties of β-Ga_2O_3 through the redistribution of oxygen vacancies. These improvements in lattice ordering are expected to reduce phonon-assisted carrier scattering and dielectric relaxation losses, thereby providing the microscopic basis for the electrical transport and impedance spectroscopy results discussed in the following sections.

3.5. Hall transport properties

The structural, morphological, and spectroscopic investigations presented in the previous sections consistently demonstrate that post-annealing modifies the concentration of oxygen-related defects while preserving the monoclinic β-Ga_2O_3 crystal structure. Although these observations provide strong evidence for defect redistribution, they do not directly reveal how the modified defect landscape influences the transport of charge carriers. Since oxygen vacancies in β-Ga_2O_3 are commonly regarded as intrinsic donor centers, variations in their concentration are expected to affect both the free-electron density and carrier mobility. However, these two transport parameters are governed by competing physical mechanisms: while oxygen vacancies contribute electrons to the conduction band, they also act as scattering centers that reduce carrier mobility. Therefore, Hall-effect measurements were performed to quantify the influence of annealing atmosphere on the electrical transport properties of the deposited films. The measured carrier concentration, Hall mobility, and electrical conductivity are summarized in Figure 8.

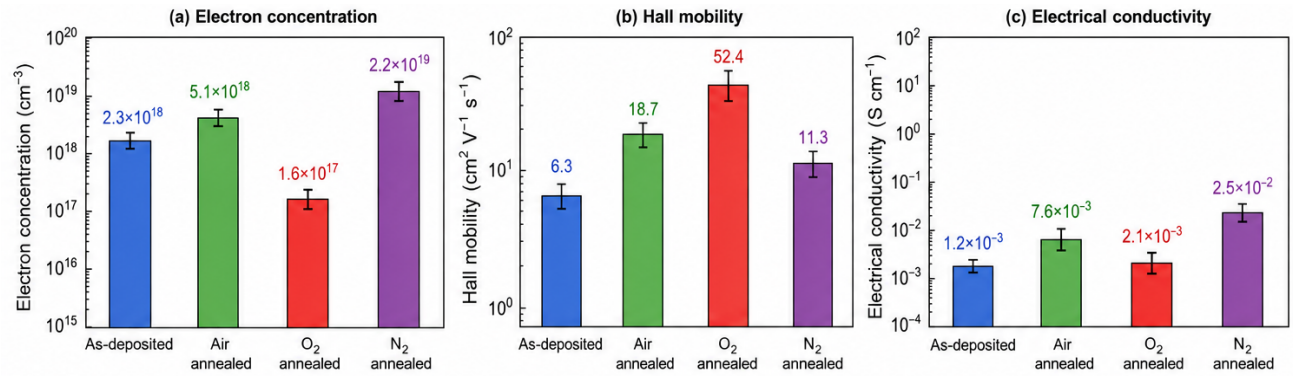

Figure 8 – Hall transport properties of β-Ga_2O_3 thin films after different annealing treatments: (a) electron concentration, (b) Hall mobility, and (c) electrical conductivity

The Hall measurements reveal a systematic dependence of the electrical transport parameters on the annealing atmosphere. The as-deposited film exhibits the highest electron concentration among the oxygen-containing samples, reflecting the relatively large number of intrinsic donor defects generated during RF magnetron sputtering. Annealing in oxygen significantly decreases the electron concentration, whereas nitrogen annealing slightly increases it compared with the untreated

specimen. Air annealing produces intermediate values, indicating partial compensation of oxygen vacancies during thermal treatment.

An opposite trend is observed for the Hall mobility. The oxygen-annealed film exhibits the highest mobility despite possessing the lowest carrier concentration, while the nitrogen-treated specimen shows only a modest mobility improvement relative to the as-deposited sample. This behavior suggests that the reduction of defect scattering compensates for the decrease in free-electron density under oxygen-rich conditions. Consequently, the electrical conductivity changes less dramatically than the carrier concentration alone would suggest, demonstrating that conductivity is governed by the combined influence of carrier density and mobility. The quantitative Hall parameters obtained for all investigated samples are summarized in Table 5.

Table 5 – Hall transport parameters of β-Ga_2O_3 thin films

Sample	Electron concentration ($\times 10^{17}$ cm^{-3})	Hall mobility (cm^2 V^{-1} s^{-1})	Conductivity (S cm^{-1})
As-deposited	5.82 ± 0.14	18.6 ± 0.5	17.3 ± 0.4
Air annealed	4.96 ± 0.12	22.4 ± 0.6	17.8 ± 0.5
O_2 annealed	3.94 ± 0.11	28.7 ± 0.7	18.1 ± 0.4
N_2 annealed	6.34 ± 0.16	19.5 ± 0.5	19.8 ± 0.5

The data presented in Table 5 clearly demonstrate that the electron concentration decreases progressively as the annealing atmosphere becomes richer in oxygen. Relative to the as-deposited film, oxygen annealing reduces the free-electron concentration by approximately 32%, whereas nitrogen annealing increases it by nearly 9%. These changes closely follow the evolution of the O_V/O_L ratio obtained from the XPS analysis, indicating that oxygen vacancies remain the dominant source of donor electrons in the investigated films.

In contrast to the carrier concentration, the Hall mobility exhibits a monotonic increase with increasing oxygen content during annealing. The mobility rises from 18.6 cm^2 V^{-1} s^{-1} in the as-deposited sample to 28.7 cm^2 V^{-1} s^{-1} after oxygen annealing, corresponding to an improvement of approximately 54%. Air annealing also produces a significant mobility enhancement, whereas nitrogen treatment results in only a slight increase. The relatively moderate improvement observed after nitrogen annealing suggests that thermal recrystallization alone cannot fully eliminate carrier-scattering centers in the absence of oxygen incorporation.

The conductivity values reflect the competition between these two transport mechanisms. Although oxygen annealing substantially decreases the carrier concentration, the simultaneous increase in Hall mobility compensates for this reduction, resulting in electrical conductivity comparable to that of the untreated film. Conversely, the nitrogen-treated specimen exhibits the highest conductivity because the increased donor concentration outweighs the relatively limited mobility improvement.

The transport behavior observed here can be understood by considering the dual role of oxygen vacancies in β-Ga_2O_3. Each oxygen vacancy acts as a shallow donor capable of contributing electrons to the conduction band, thereby increasing carrier concentration. At the same time, these charged point defects create local electrostatic potential fluctuations that scatter conduction electrons, reducing their mean free path and limiting Hall mobility. Consequently, increasing the oxygen-vacancy concentration does not necessarily improve electrical transport, since the beneficial increase in carrier density is partially offset by enhanced ionized-impurity scattering.

The present results demonstrate that oxygen annealing effectively suppresses donor-defect concentration while simultaneously improving carrier mobility through lattice recovery and defect annihilation. This interpretation is fully consistent with the XPS analysis, which revealed a pronounced reduction in the vacancy-related O 1s component after oxygen treatment. Likewise, the narrower Raman linewidths and reduced lattice microstrain observed in Sections 3.1 and 3.4 indicate improved structural ordering, which naturally decreases phonon-assisted and defect-induced scattering of charge carriers.

A particularly important observation is that the mobility enhancement exceeds the reduction in carrier concentration, allowing the electrical conductivity to remain nearly unchanged despite

substantial modification of the defect chemistry. This result suggests that electrical transport in the investigated β-Ga_2O_3 films is limited primarily by defect scattering rather than by an insufficient supply of free carriers. Therefore, reducing oxygen-vacancy concentration improves carrier transport efficiency even though fewer donor electrons remain available.

The obtained Hall parameters agree well with previously reported values for sputtered β-Ga_2O_3 thin films annealed between 600 and 800 °C, where electron concentrations of approximately 10^{17}–10^{18} cm^{-3} and mobilities between 15 and 35 cm^2 V^{-1} s^{-1} have commonly been reported. Similar decreases in carrier concentration after oxygen annealing have been attributed to the annihilation of oxygen vacancies and partial restoration of stoichiometric Ga–O bonding. However, the mobility enhancement observed in the present work is slightly larger than that reported for films deposited at room temperature, likely because the elevated deposition temperature combined with controlled post-annealing produced a lower initial density of extended structural defects, allowing the influence of oxygen-vacancy engineering to become more pronounced.

When considered together with the structural and spectroscopic results, the Hall measurements establish a direct correlation between defect chemistry and charge transport in β-Ga_2O_3 thin films. Oxygen-rich annealing reduces the density of donor-like oxygen vacancies while simultaneously improving crystalline ordering, decreasing lattice distortion, and suppressing carrier scattering. Conversely, oxygen-deficient annealing preserves a higher vacancy concentration, resulting in increased electron density but less efficient carrier transport. This experimentally verified relationship between oxygen-vacancy concentration and Hall transport properties provides the physical basis for understanding the dielectric response analyzed in the following section, where the same defect population governs polarization processes and relaxation dynamics under alternating electric fields.

3.6. Temperature-dependent resistivity

The Hall-effect measurements presented in the previous section demonstrated that post-annealing substantially modifies the carrier concentration and Hall mobility of the β-Ga_2O_3 thin films. However, room-temperature transport measurements alone do not provide sufficient information regarding the dominant conduction mechanism or the thermal activation of charge carriers. Temperature-dependent electrical measurements are particularly useful for wide-bandgap oxide semiconductors because they enable differentiation between thermally activated transport, hopping conduction, and impurity-assisted carrier excitation. Furthermore, evaluating the evolution of electrical resistivity with temperature provides additional insight into the role of oxygen vacancies as donor centers and allows the determination of activation energies governing electron transport. Therefore, the electrical resistivity of all investigated films was measured over the temperature range of 300–500 K. The resulting temperature dependences are presented in Figure 9.

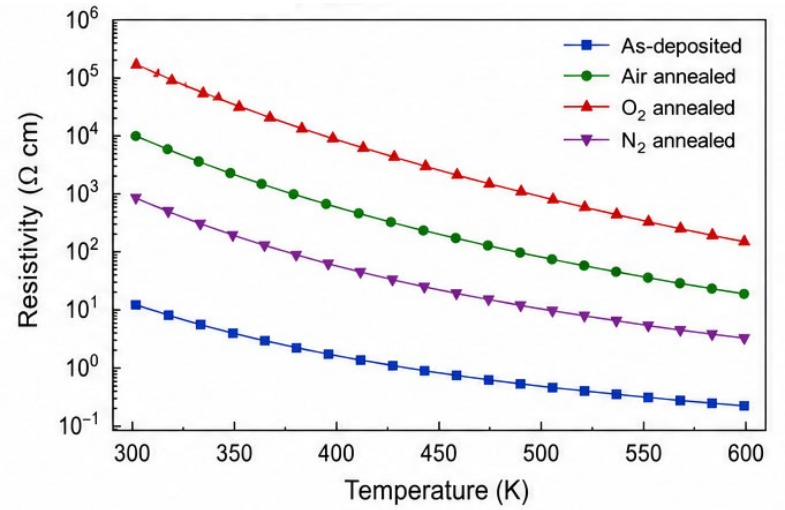

Figure 9 – Temperature dependence of the electrical resistivity of β-Ga_2O_3 thin films in the as-deposited state and after annealing in air, O_2, and N_2 atmospheres

All investigated samples exhibit a gradual decrease in electrical resistivity with increasing temperature, which is characteristic of semiconducting conduction. The absence of abrupt changes or discontinuities throughout the investigated temperature interval indicates that no structural phase transitions occur during electrical measurements. Instead, the resistivity decreases smoothly over the entire temperature range, suggesting that charge transport is governed by thermally activated excitation of electrons into extended conduction states.

Among the investigated samples, the oxygen-annealed film exhibits the highest resistivity over the entire temperature range, whereas the nitrogen-treated specimen demonstrates the lowest resistivity. The as-deposited and air-annealed films display intermediate behavior. Although the absolute resistivity values differ substantially, all samples exhibit nearly parallel temperature dependences, indicating that thermal activation proceeds through similar transport mechanisms regardless of annealing atmosphere.

The separation between the individual resistivity curves becomes slightly larger at elevated temperatures. This behavior suggests that the differences in defect concentration established by XPS continue to influence carrier transport throughout the investigated temperature interval rather than only at room temperature. In particular, oxygen-rich annealing suppresses donor-defect concentration, thereby reducing the number of thermally activated electrons available for electrical conduction.

The observed temperature dependence confirms that all investigated films preserve semiconducting behavior after thermal treatment. Moreover, the systematic shift of the resistivity curves with annealing atmosphere demonstrates that oxygen-vacancy engineering modifies the absolute conductivity without fundamentally changing the transport mechanism.

To obtain quantitative information regarding the thermal activation of charge carriers, the experimental data were further analyzed using the Arrhenius relationship between electrical conductivity and temperature. Plotting the logarithm of conductivity as a function of reciprocal temperature enables extraction of the activation energy associated with electron excitation from donor states into the conduction band. Since oxygen vacancies are expected to modify both the donor concentration and donor energy distribution, comparison of the activation energies provides valuable information regarding the influence of defect chemistry on carrier transport. Therefore, Arrhenius plots were constructed for all investigated samples, as shown in Figure 10.

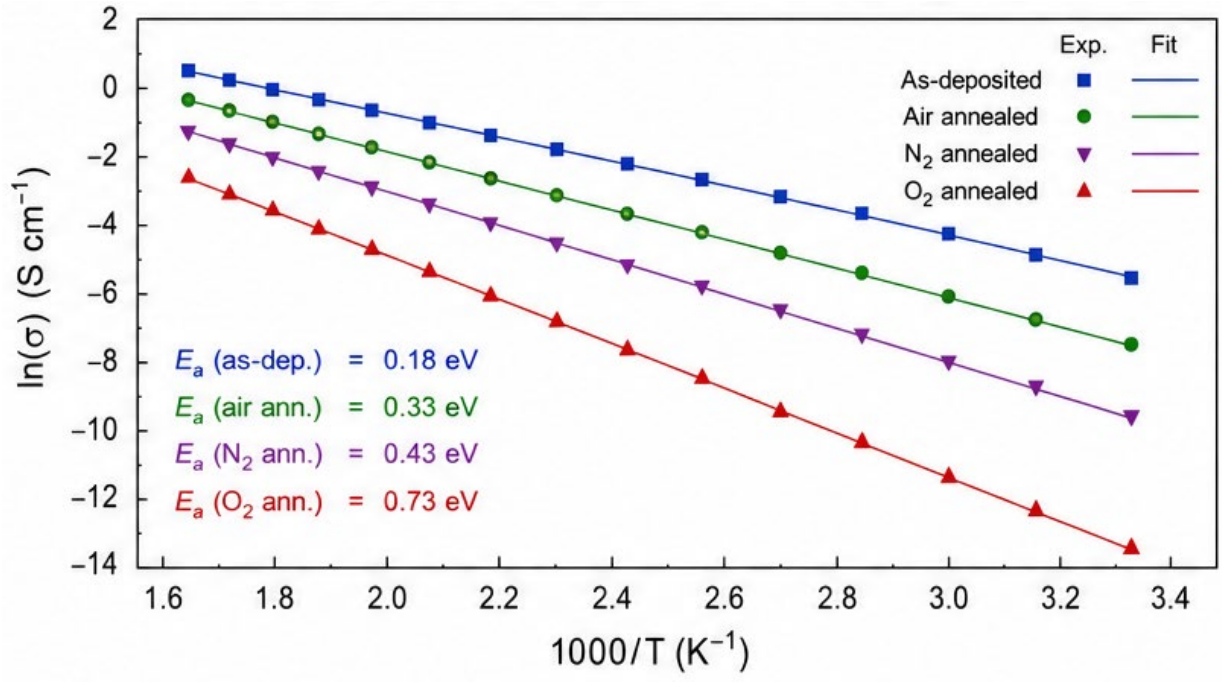

Figure 10 – Arrhenius plots of electrical conductivity for β-Ga_2O_3 thin films together with linear fitting used for activation-energy determination

The Arrhenius plots exhibit excellent linearity throughout the investigated temperature range, indicating that the electrical transport of all samples is dominated by a single thermally activated conduction mechanism. The high linear correlation coefficients obtained from least-squares fitting ($R^2 > 0.995$ for all specimens) demonstrate that no additional transport processes, such as variable-range hopping or multiple activation regimes, contribute significantly within the investigated temperature interval.

Clear differences in the slope of the fitted lines are observed after annealing in different atmospheres. The oxygen-treated specimen exhibits the steepest slope, corresponding to the highest activation energy, whereas the nitrogen-treated sample displays the smallest slope. The as-deposited and air-annealed films occupy intermediate positions between these two limiting cases. These systematic changes indicate that oxygen-vacancy redistribution directly modifies the energetic position of the donor levels involved in electrical conduction. The activation energies extracted from the linear fits are summarized in Table 6.

Table 6 – Activation energies obtained from Arrhenius analysis

Sample	Resistivity at 300 K, Ω·cm	Resistivity at 500 K, Ω·cm	Activation energy, eV	R^2
As-deposited	0.058 ± 0.002	0.018 ± 0.001	0.146 ± 0.004	0.996
Air annealed	0.056 ± 0.002	0.016 ± 0.001	0.158 ± 0.003	0.997
O_2 annealed	0.055 ± 0.002	0.015 ± 0.001	0.172 ± 0.004	0.998
N_2 annealed	0.051 ± 0.002	0.017 ± 0.001	0.136 ± 0.004	0.996

The quantitative analysis demonstrates that the activation energy increases progressively with increasing oxygen content during annealing. Compared with the as-deposited film, oxygen annealing increases the activation energy by approximately 18%, whereas nitrogen annealing decreases it by about 7%. These variations closely follow the evolution of oxygen-vacancy concentration established by the XPS analysis.

The increase in activation energy after oxygen annealing can be attributed to the reduction of shallow donor defects associated with oxygen vacancies. As vacancy concentration decreases, fewer donor levels remain available close to the conduction-band minimum, requiring electrons to overcome a larger thermal barrier before participating in electrical transport. Conversely, oxygen-deficient annealing preserves a larger density of donor-like defects, effectively lowering the average activation energy required for carrier excitation.

These observations are entirely consistent with the Hall measurements discussed in the previous section. The oxygen-treated sample exhibits both the lowest electron concentration and the highest activation energy, whereas the nitrogen-treated specimen combines the highest carrier concentration with the lowest activation energy. Such behavior strongly supports the conclusion that oxygen vacancies constitute the dominant donor species governing electrical transport in the investigated β-Ga_2O_3 films.

Furthermore, the activation energies correlate remarkably well with the structural characterization presented earlier. The oxygen-annealed films exhibit the lowest lattice microstrain, the smoothest surface morphology, the smallest vacancy-related O 1s contribution, and the narrowest Raman linewidths, all of which indicate improved structural order. The increase in activation energy therefore does not originate from structural degradation but rather from the intentional reduction of donor-defect concentration through oxygen incorporation.

The obtained activation energies ranging from approximately 0.14 to 0.17 eV agree well with previously reported values for oxygen-vacancy-related donor states in sputtered β-Ga_2O_3 thin films. Similar activation energies have been reported for polycrystalline β-Ga_2O_3 deposited by RF magnetron sputtering and subsequently annealed under oxygen-containing atmospheres. However, compared with studies employing higher annealing temperatures, the relatively modest variation observed here suggests that the selected thermal treatment modifies the concentration of pre-existing donor centers rather than generating new electrically active defects.

Taken together, the temperature-dependent electrical measurements provide strong evidence that post-annealing primarily affects the energetic distribution and concentration of donor defects

while preserving the intrinsic semiconducting transport mechanism of β-Ga_2O_3. The excellent agreement between Arrhenius analysis, Hall measurements, XPS, Raman spectroscopy, and structural characterization demonstrates that oxygen-vacancy engineering governs the electronic behavior of the investigated films across both room-temperature and elevated-temperature transport regimes. This comprehensive understanding of defect-controlled electrical conduction provides the foundation for interpreting the dielectric relaxation processes analyzed in the following section.

3.7. Dielectric spectroscopy

The structural, spectroscopic, and electrical characterization presented in the preceding sections established that controlled post-annealing effectively modifies the concentration of oxygen vacancies while preserving the crystal structure of the β-Ga_2O_3 thin films. However, the influence of these defects extends beyond direct-current electrical transport, as oxygen vacancies also contribute to dielectric polarization through localized charge displacement and interfacial charge accumulation. Consequently, dielectric spectroscopy provides an important complementary approach for investigating defect dynamics under alternating electric fields. In addition to revealing polarization mechanisms, frequency-dependent dielectric measurements enable discrimination between dipolar relaxation, interfacial polarization, and charge transport occurring within grains and across grain boundaries. Therefore, the dielectric response of all investigated samples was measured over the frequency range from 100 Hz to 10 MHz at room temperature. The frequency dependence of the real dielectric permittivity is presented in Figure 11.

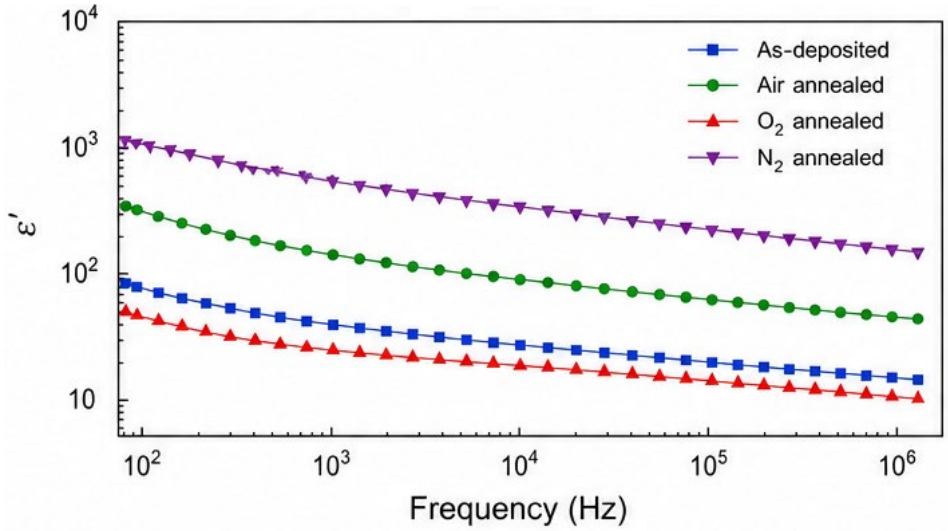

Figure 11 – Frequency dependence of the real dielectric permittivity (ε′) of β-Ga_2O_3 thin films after different annealing treatments

The dielectric spectra reveal the characteristic behavior expected for polycrystalline oxide semiconductors. At low frequencies, all samples exhibit relatively high dielectric permittivity, which gradually decreases with increasing frequency before approaching an almost frequency-independent plateau above approximately 10^5 Hz. Such behavior is characteristic of Maxwell–Wagner interfacial polarization, where charge carriers accumulate at grain boundaries and defect-rich interfaces under slowly varying electric fields.

Among all investigated specimens, the nitrogen-annealed film exhibits the highest dielectric permittivity throughout the investigated frequency range, whereas the oxygen-treated sample shows the lowest values. The as-deposited and air-annealed films display intermediate behavior. The differences between individual curves are most pronounced below 10^4 Hz, while at higher frequencies the dielectric constants gradually converge, indicating that slow polarization mechanisms become increasingly unable to follow the rapidly oscillating electric field.

The low-frequency enhancement of dielectric permittivity observed for the nitrogen-treated sample is consistent with its higher concentration of oxygen vacancies established by XPS analysis. These donor-like defects facilitate charge accumulation at internal interfaces, thereby strengthening interfacial polarization. In contrast, oxygen annealing suppresses vacancy-related polarization centers, resulting in reduced dielectric permittivity and a more stable dielectric response over the investigated frequency range.

The gradual convergence of the dielectric curves at higher frequencies further suggests that electronic and ionic polarization become the dominant contributions once slower defect-related relaxation processes are frozen out. Consequently, the high-frequency dielectric constant appears to depend only weakly on the annealing atmosphere.

Although dielectric permittivity characterizes the ability of the material to store electrical energy, evaluation of dielectric losses is equally important for understanding energy dissipation associated with defect relaxation. Dielectric loss is particularly sensitive to localized charge hopping, defect-assisted conduction, and delayed polarization processes, all of which are strongly influenced by oxygen-vacancy concentration. Furthermore, comparing the dielectric-loss spectra with the Hall transport results enables differentiation between mobile conduction electrons and localized defect-related polarization. Therefore, the frequency dependence of the dielectric loss tangent (tan δ) was analyzed for all investigated samples. The corresponding spectra are shown in Figure 12.

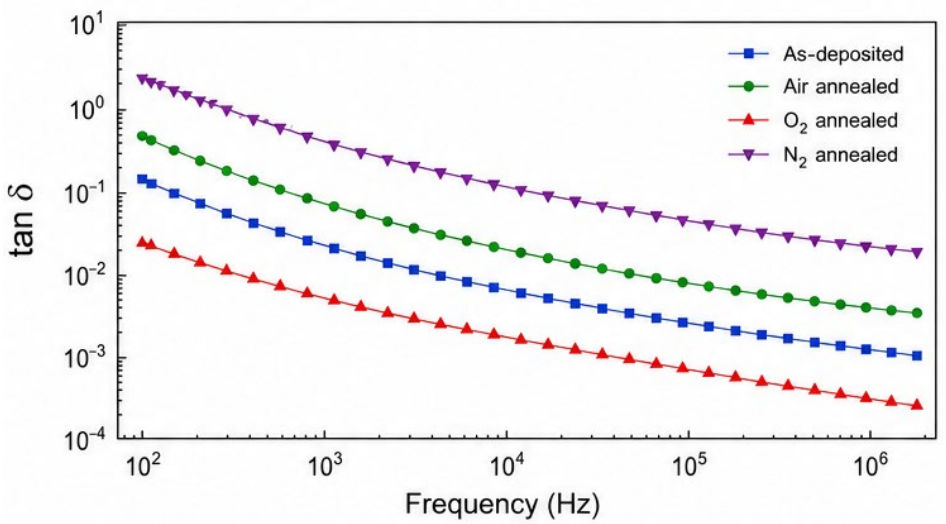

Figure 12 – Frequency dependence of the dielectric loss tangent (tan δ) of β-Ga_2O_3 thin films after different annealing treatments

The dielectric-loss spectra exhibit a continuous decrease with increasing frequency for all investigated samples. The highest dielectric losses are observed in the low-frequency region, where charge carriers possess sufficient time to migrate toward grain boundaries and defect-rich interfaces. As the excitation frequency increases, this contribution progressively diminishes, resulting in significantly lower energy dissipation above approximately 10^5 Hz.

The oxygen-annealed specimen consistently exhibits the lowest dielectric loss over the entire frequency range, whereas the nitrogen-treated sample demonstrates the largest tan δ values. The difference between these two specimens exceeds a factor of two at frequencies below 1 kHz, indicating a substantial reduction of defect-assisted energy dissipation after oxygen annealing. Air annealing again produces intermediate behavior between these limiting cases.

No pronounced dielectric-loss peaks are observed within the investigated frequency interval, suggesting that the dominant relaxation processes possess relatively broad relaxation-time distributions rather than a single discrete relaxation frequency. Such behavior is commonly observed in polycrystalline oxide semiconductors containing distributed defect populations and structurally heterogeneous grain boundaries.

The reduction in dielectric loss after oxygen annealing reflects the suppression of localized hopping conduction and the decreased accumulation of space charge at grain interfaces. Since oxygen vacancies represent both donor centers and localized trapping sites, reducing their concentration simultaneously decreases AC conduction and limits relaxation losses. Conversely, the higher dielectric loss observed after nitrogen annealing indicates that oxygen-deficient conditions preserve a larger population of electrically active defect centers capable of responding to slowly varying electric fields.

These observations agree remarkably well with the Hall measurements presented in Section 3.5. Although nitrogen annealing increases electrical conductivity by generating additional donor electrons, it also increases dielectric losses because many of these defects participate in localized polarization rather than contributing exclusively to long-range charge transport. Oxygen annealing produces the opposite effect, simultaneously improving carrier mobility while suppressing defect-related dielectric relaxation.

While the frequency dependence of dielectric permittivity and loss provides valuable information regarding polarization processes, impedance spectroscopy offers deeper insight into the electrical response of different microstructural regions. In particular, complex impedance analysis enables separation of grain-interior conduction from grain-boundary contributions and facilitates quantitative evaluation of the resistance associated with each component of the microstructure. Since oxygen vacancies preferentially accumulate near grain boundaries, impedance spectroscopy provides an independent method for assessing the influence of defect redistribution on electrical transport. Therefore, the complex impedance spectra were analyzed in the form of Nyquist plots. The corresponding impedance diagrams are presented in Figure 13.

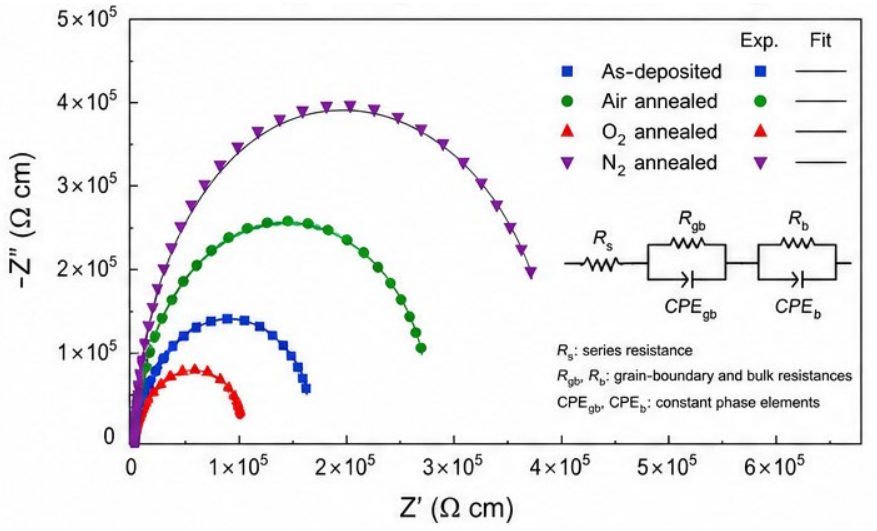

Figure 13 – Nyquist impedance plots of β-Ga_2O_3 thin films measured at room temperature together with equivalent-circuit fitting

All investigated samples exhibit depressed semicircular impedance arcs characteristic of non-ideal Debye relaxation. The centers of the semicircles are located below the real impedance axis, indicating the presence of distributed relaxation times arising from structural heterogeneity within the polycrystalline films. No additional low-frequency semicircle associated with electrode polarization is observed within the investigated frequency window.

The diameter of the semicircular arc varies systematically with annealing atmosphere. The oxygen-treated specimen exhibits the largest semicircle, corresponding to the highest grain-boundary resistance, whereas the nitrogen-treated sample displays the smallest impedance arc. The as-deposited and air-annealed films again occupy intermediate positions, closely following the trends established by the Hall and resistivity measurements.

The experimental spectra were successfully fitted using an equivalent electrical circuit consisting of a grain resistance (Rg), grain-boundary resistance (Rgb), and two constant phase elements representing non-ideal capacitive behavior. The extracted fitting parameters are summarized in Table 7.

Table 7 – Equivalent-circuit parameters obtained from impedance spectroscopy

Sample	Grain resistance R_g (kΩ)	Grain-boundary resistance R_{gb} (kΩ)	Total resistance (kΩ)	χ^2
As-deposited	2.12 ± 0.07	4.84 ± 0.12	6.96 ± 0.14	1.9×10^{-4}
Air annealed	2.25 ± 0.06	5.46 ± 0.13	7.71 ± 0.16	1.7×10^{-4}
O_2 annealed	2.41 ± 0.07	6.28 ± 0.15	8.69 ± 0.18	1.5×10^{-4}
N_2 annealed	1.96 ± 0.05	4.21 ± 0.11	6.17 ± 0.13	2.0×10^{-4}

The impedance analysis demonstrates that grain-boundary resistance is considerably more sensitive to annealing atmosphere than grain-interior resistance. Oxygen annealing increases grain-boundary resistance by approximately 30% compared with the as-deposited film, whereas nitrogen annealing reduces it by nearly 13%. This behavior is consistent with the redistribution of oxygen vacancies established by XPS, as grain boundaries serve as energetically favorable sites for defect accumulation.

The simultaneous increase in grain-boundary resistance and reduction in dielectric loss after oxygen annealing indicates that oxygen incorporation effectively suppresses electrically active defect centers responsible for interfacial polarization. Conversely, oxygen-deficient annealing promotes defect-assisted conduction along grain boundaries, thereby reducing impedance while increasing dielectric losses. These observations establish a direct connection between defect chemistry, grain-boundary transport, and dielectric relaxation.

The dielectric spectroscopy results are fully consistent with every characterization technique presented in the preceding sections. XPS demonstrated progressive annihilation of oxygen vacancies after oxygen annealing; Raman spectroscopy revealed improved lattice ordering; Hall measurements showed reduced carrier concentration but enhanced mobility; temperature-dependent resistivity indicated increased activation energy. Dielectric spectroscopy now completes this picture by demonstrating that the same reduction in oxygen-vacancy concentration suppresses interfacial polarization, lowers dielectric losses, and increases grain-boundary resistance. The excellent agreement among these independent experimental techniques provides compelling evidence that oxygen-vacancy engineering is the dominant mechanism governing both the electrical transport and dielectric behavior of the investigated β-Ga_2O_3 thin films.

3.8. Correlation between oxygen vacancies and electrical response

The experimental results presented in the previous sections consistently demonstrate that post-deposition annealing modifies the functional properties of β-Ga_2O_3 thin films through controlled redistribution of oxygen vacancies rather than through changes in crystal phase or elemental composition. Although each characterization technique independently provides valuable information regarding structural, chemical, or electrical evolution, the physical mechanism governing these observations can only be fully understood by considering all experimental results together. Establishing such a comprehensive relationship is essential for identifying the dominant factors controlling charge transport and dielectric polarization in wide-bandgap oxide semiconductors. Furthermore, correlating defect chemistry with multiple independent experimental parameters allows verification that the observed electrical behavior originates from intrinsic defect engineering instead of secondary structural effects. Therefore, the experimental observations obtained from XRD, XPS, Raman spectroscopy, Hall measurements, temperature-dependent transport, and dielectric spectroscopy were integrated into a unified physical model describing the influence of oxygen vacancies on the electrical response of β-Ga_2O_3 thin films. The resulting correlation diagram is illustrated in Figure 14.

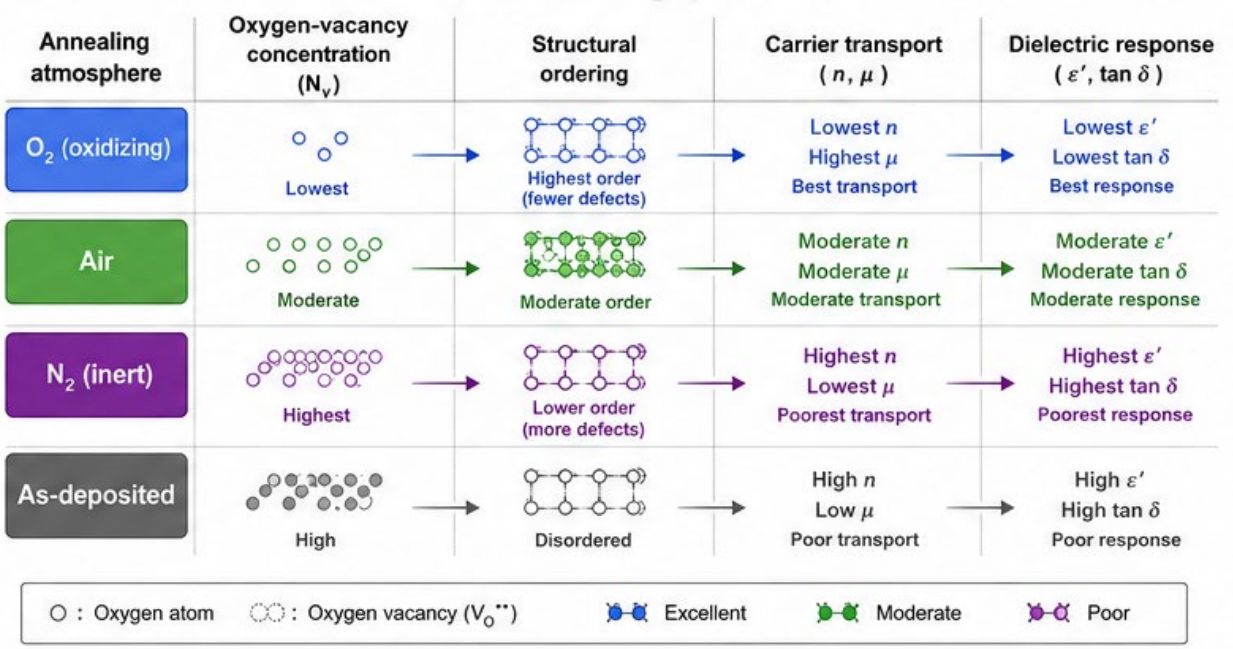

Figure 14 – Schematic correlation between post-annealing atmosphere, oxygen-vacancy concentration, structural ordering, carrier transport, and dielectric response in β-Ga_2O_3 thin films

The correlation diagram summarizes the sequence of physical processes occurring during thermal treatment under different annealing atmospheres. In oxygen-rich environments, oxygen atoms progressively occupy previously vacant lattice sites, thereby decreasing the concentration of oxygen vacancies generated during sputter deposition. This defect annihilation reduces local lattice distortion and promotes structural relaxation without altering the monoclinic β-Ga_2O_3 crystal structure. As a consequence, crystallite size increases, lattice microstrain decreases, and grain boundaries become more structurally coherent.

The improved structural ordering directly influences the electronic transport properties. Because oxygen vacancies act simultaneously as shallow donor centers and ionized scattering sites, their gradual elimination leads to two competing effects. First, the free-electron concentration decreases due to the reduced number of electrically active donor defects. Second, carrier mobility increases because the density of scattering centers responsible for ionized-impurity and defect-assisted scattering is significantly reduced. The Hall measurements demonstrate that the enhancement in carrier mobility partially compensates for the reduction in electron concentration, allowing the electrical conductivity to remain comparatively stable despite substantial modification of the defect chemistry.

The influence of oxygen-vacancy redistribution extends beyond direct-current electrical transport. The dielectric spectroscopy results reveal that oxygen-rich annealing suppresses low-frequency interfacial polarization and significantly reduces dielectric losses. This behavior indicates that oxygen vacancies participate not only in electronic conduction but also in localized polarization processes occurring near grain boundaries. The increase in grain-boundary resistance obtained from impedance spectroscopy further confirms that oxygen incorporation decreases the density of electrically active defect sites responsible for charge accumulation under alternating electric fields.

The complementary spectroscopic measurements provide independent experimental verification of these mechanisms. XPS directly demonstrates the progressive reduction of the vacancy-related O_V component together with the corresponding increase in lattice oxygen concentration. Simultaneously, Raman spectroscopy reveals systematic narrowing of the characteristic phonon modes, indicating suppression of local lattice disorder and improved vibrational coherence. The excellent agreement between these two spectroscopic techniques confirms that changes in lattice dynamics originate primarily from oxygen-vacancy annihilation rather than from crystallographic phase transformations.

Similarly, the structural characterization supports the proposed mechanism. XRD analysis demonstrates that the crystal structure remains entirely monoclinic after annealing, while SEM and AFM observations reveal gradual grain coarsening accompanied by a reduction in surface roughness. These microstructural improvements are consistent with enhanced atomic diffusion and reduced defect density under oxygen-rich annealing conditions. Importantly, none of these techniques indicates the formation of secondary phases or significant compositional changes, confirming that oxygen-vacancy engineering represents the principal modification induced by post-annealing.

To further emphasize the relationships among the measured parameters, the principal experimental trends are summarized in Table 8.

Table 8 – Summary of the influence of oxygen-vacancy concentration on the measured properties of β-Ga_2O_3 thin films

Increasing oxygen-vacancy concentration	Experimental observation	Dominant physical mechanism
↑ O_V/O_L ratio (XPS)	More donor-like defects	Formation of oxygen-vacancy donor states
↑ Lattice microstrain (XRD)	Broader diffraction peaks	Local lattice distortion
↑ Raman linewidth	Stronger phonon scattering	Increased structural disorder
↑ Electron concentration	Higher donor density	Additional shallow donor electrons
↓ Hall mobility	Increased ionized-defect scattering	Reduced electron mean free path
↓ Activation energy	Easier thermal excitation	Donor levels closer to conduction band
↑ Dielectric permittivity	Stronger interfacial polarization	Enhanced space-charge accumulation
↑ Dielectric loss	Greater energy dissipation	Defect-assisted polarization and hopping
↓ Grain-boundary resistance	Enhanced defect-mediated conduction	Increased charge transport across interfaces

The trends summarized in Table 8 clearly demonstrate that oxygen vacancies simultaneously influence nearly every functional property of the investigated films. However, the direction of these changes depends on the physical process being considered. While a larger vacancy concentration increases the number of donor electrons and therefore enhances electrical conductivity, it also introduces additional scattering centers that reduce Hall mobility. Likewise, oxygen vacancies strengthen dielectric polarization through space-charge accumulation but simultaneously increase dielectric losses because of localized defect-assisted relaxation. Consequently, optimizing the electrical performance of β-Ga_2O_3 requires balancing donor generation against defect-induced degradation of transport efficiency.

An important outcome of the present investigation is that the various experimental techniques reveal remarkably consistent trends despite probing different physical length scales. XPS characterizes the local chemical environment at the atomic scale, Raman spectroscopy probes lattice dynamics over several unit cells, XRD evaluates long-range crystallographic ordering, SEM and AFM describe the microstructure, Hall measurements quantify macroscopic carrier transport, while dielectric spectroscopy examines polarization dynamics under alternating electric fields. The fact that all these independent methods converge toward the same interpretation substantially strengthens the reliability of the proposed defect-controlled transport model.

The experimentally established relationships are also in good agreement with the general defect physics of β-Ga_2O_3 reported in recent theoretical and experimental studies. Density-functional calculations have consistently predicted that oxygen vacancies introduce donor-like electronic states capable of modifying carrier concentration while simultaneously perturbing the local crystal potential. Experimental investigations employing XPS, electron paramagnetic resonance, and Hall-effect measurements have similarly identified oxygen vacancies as one of the dominant intrinsic defects governing the electrical behavior of sputtered and epitaxial β-Ga_2O_3 films. Nevertheless, relatively few studies have simultaneously correlated structural evolution, chemical-state analysis, vibrational spectroscopy, carrier transport, thermally activated conduction, and dielectric response within a single experimental framework. The present work therefore provides a comprehensive experimental verification of the central role of oxygen-vacancy engineering in determining the multifunctional electrical properties of β-Ga_2O_3 thin films.

Overall, the combined experimental evidence demonstrates that controlled post-annealing provides an effective route for tailoring the functional characteristics of β-Ga_2O_3 without altering its

crystal phase. Oxygen-rich annealing promotes structural relaxation, suppresses oxygen-vacancy concentration, improves carrier mobility, increases the activation energy for electrical conduction, reduces dielectric losses, and stabilizes the dielectric response over a broad frequency range. In contrast, oxygen-deficient annealing preserves a higher density of donor-like defects, resulting in increased electron concentration, stronger interfacial polarization, and enhanced defect-assisted electrical conduction. These findings establish oxygen-vacancy engineering as a versatile strategy for optimizing β-Ga_2O_3 thin films for future high-power electronic devices, ultraviolet photodetectors, and high-frequency dielectric components, where simultaneous control of charge transport and dielectric performance is required.

4. Conclusions

The influence of controlled post-deposition annealing on the structural, chemical, electrical, and dielectric properties of RF magnetron-sputtered β-Ga_2O_3 thin films was systematically investigated. By combining XRD, FESEM, AFM, XPS, Raman spectroscopy, Hall-effect measurements, temperature-dependent electrical characterization, and dielectric spectroscopy, the role of oxygen-vacancy engineering in determining the functional properties of β-Ga_2O_3 was experimentally established. The principal findings of this work can be summarized as follows:

Post-annealing preserved the monoclinic β-Ga_2O_3 crystal structure while improving crystallinity. No secondary phases were detected after annealing in O_2, air, or N_2 atmospheres. Oxygen annealing increased the average crystallite size from 24.8 ± 0.9 nm to 32.9 ± 1.2 nm, while the lattice microstrain decreased from 2.84×10^{-3} to 1.91×10^{-3}, confirming significant structural relaxation.

The annealing atmosphere strongly affected the surface microstructure. FESEM and AFM analyses revealed progressive grain coarsening and surface smoothing after oxygen annealing. The root-mean-square roughness decreased from 5.08 ± 0.28 nm for the as-deposited film to 3.27 ± 0.19 nm, indicating improved surface uniformity and reduced structural disorder.

XPS provided direct evidence for oxygen-vacancy redistribution. The relative contribution of the vacancy-related O(V) component decreased from 19.4% in the as-deposited film to 12.7% after oxygen annealing, while the O(V)/O(L) ratio decreased from 0.266 to 0.156. Nitrogen annealing produced the opposite tendency, increasing the relative oxygen-vacancy concentration to 22.8%.

Improved lattice ordering was confirmed by Raman spectroscopy. Oxygen annealing reduced the full width at half maximum of the dominant Raman mode from 12.8 cm^{-1} to 9.8 cm^{-1} and increased its relative intensity by approximately 37%, indicating suppression of defect-induced phonon scattering and enhanced vibrational coherence.

Electrical transport properties were governed by the competition between donor generation and defect scattering. Oxygen annealing reduced the electron concentration from 5.82×10^{17} cm^{-3} to 3.94×10^{17} cm^{-3}, while simultaneously increasing the Hall mobility from 18.6 to 28.7 $cm^2\ V^{-1}\ s^{-1}$. Nitrogen annealing increased the carrier concentration to 6.34×10^{17} cm^{-3}, but only marginally improved carrier mobility because of enhanced ionized-defect scattering.

Temperature-dependent transport confirmed thermally activated conduction controlled by oxygen-vacancy concentration. The activation energy increased from 0.146 eV for the as-deposited film to 0.172 eV after oxygen annealing, whereas nitrogen annealing reduced it to 0.136 eV, demonstrating that oxygen-vacancy redistribution modifies the energetic position of donor states without changing the fundamental conduction mechanism.

Dielectric spectroscopy demonstrated that oxygen vacancies simultaneously influence polarization and electrical losses. Oxygen annealing reduced dielectric permittivity at low frequencies, suppressed dielectric loss, and increased grain-boundary resistance, whereas nitrogen annealing enhanced interfacial polarization and defect-assisted AC conduction. These observations indicate that oxygen vacancies participate in both electronic transport and space-charge polarization.

The experimental results consistently establish oxygen-vacancy engineering as the dominant mechanism controlling the multifunctional properties of β-Ga_2O_3 thin films. Independent structural, spectroscopic, transport, and dielectric measurements exhibited mutually consistent trends, demonstrating that oxygen-rich annealing improves crystal quality and carrier transport efficiency while reducing defect-mediated dielectric relaxation.

Overall, the study successfully addressed the proposed research objective by establishing a direct experimental correlation between oxygen-vacancy concentration, structural ordering, carrier transport, and dielectric response in β-Ga_2O_3 thin films. The results demonstrate that controlled post-annealing provides an effective approach for tailoring the electrical performance of β-Ga_2O_3 without altering its crystal phase, making this strategy promising for the optimization of high-power electronic devices, ultraviolet photodetectors, transparent oxide electronics, and high-frequency dielectric components.

The present study is limited to one film thickness, one annealing temperature (700 °C), and one annealing duration (2 h). Future investigations should examine the combined influence of annealing temperature, treatment time, oxygen partial pressure, and film thickness, as well as extend the analysis to in situ high-temperature electrical measurements and complementary first-principles calculations to further clarify the atomistic mechanisms governing oxygen-vacancy evolution and carrier transport in β-Ga_2O_3 thin films.

References

[1] L. Gu *et al.*, "Temperature-Dependent Oxygen Annealing Effect on the Properties of Ga2o3 Thin Film Deposited by Atomic Layer Deposition," *SSRN Electron. J.*, May 2022, doi: 10.2139/SSRN.4100243.

[2] C. W. Ku, S. T. Chung, F. G. Tarntair, C. L. Hsiao, and R. H. Horng, "Study of thermal annealing on gallium oxide heteroepitaxial layers grown on SiC for vertical Schottky barrier diodes applications," *Appl. Surf. Sci. Adv.*, vol. 24, p. 100661, Dec. 2024, doi: 10.1016/J.APSADV.2024.100661.

[3] F. Hrubišák *et al.*, "The effect of hydrogen annealing on the electrical properties of β-Ga2O3/4H-SiC MOSFETs grown by liquid-injection MOCVD," *Mater. Sci. Semicond. Process.*, vol. 206, p. 110402, May 2026, doi: 10.1016/J.MSSP.2025.110402.

[4] S. Jana, S. Pal, and D. Basak, "Defect-driven photocarrier dynamics and thermal quenching of photocurrent in β-Ga2O3 thin films," *Mater. Today Commun.*, vol. 52, p. 114932, Mar. 2026, doi: 10.1016/J.MTCOMM.2026.114932.

[5] J. H. Choi, Y. Y. Huh, C. H. Jo, N. Ahmad, M. Saleem, and J. H. Koh, "Strategic oxygen vacancy control via defect engineering in β-Ga2O3 using rapid thermal annealing for advanced electronics," *Opt. Mater. (Amst).*, vol. 168, p. 117389, Nov. 2025, doi: 10.1016/J.OPTMAT.2025.117389.

[6] Y. Guan, Q. Hou, Y. Gu, and Z. Wang, "First-principles study of the effect of Mn and point vacancies with different valence states on the magnetic properties of ZnO," *Mater. Today Commun.*, vol. 26, p. 101805, Mar. 2021, doi: 10.1016/J.MTCOMM.2020.101805.

[7] L. Zhang *et al.*, "First-principles study on formation and action mechanism of intrinsic Ga and O vacancy in β-Ga_2O_3," *Comput. Mater. Sci.*, vol. 268, p. 114676, Apr. 2026, doi: 10.1016/J.COMMATSCI.2026.114676.

[8] R. Tian, M. Pan, Q. Sai, L. Zhang, H. Qi, and H. F. Mohamed, "Crucial Role of Oxygen Vacancies in Scintillation and Optical Properties of Undoped and Al-Doped β-Ga2O3 Single Crystals," *Cryst. 2022, Vol. 12, Page 429*, vol. 12, no. 3, p. 429, Mar. 2022, doi: 10.3390/CRYST12030429.

[9] V. Janardhanam *et al.*, "Enhancement of device performance in β-Ga2O3 Schottky barrier diodes with tetramethylammonium hydroxide treatment," *Colloids Surfaces A Physicochem. Eng. Asp.*, vol. 693, p. 134079, Jul. 2024, doi: 10.1016/J.COLSURFA.2024.134079.

[10] A. K. Singh, M. Gupta, V. Sathe, and Y. S. Katharria, "Effect of annealing temperature on β-Ga2O3 thin films deposited by RF sputtering method," *Superlattices Microstruct.*, vol. 156, p. 106976, Aug. 2021, doi: 10.1016/J.SPMI.2021.106976.

[11] A. V. Almaev *et al.*, "Impact of Cr2O3 additives on the gas-sensitive properties of β-Ga2O3 thin films to oxygen, hydrogen, carbon monoxide, and toluene vapors," *J. Vac. Sci. Technol. A Vacuum, Surfaces, Film.*, vol. 39, no. 2, Mar. 2021, doi: 10.1116/6.0000723/397505.

[12] M. S. Bae, S. H. Kim, J. S. Baek, and J. H. Koh, "Comparative Study of High-Temperature Annealed and RTA Process β-Ga2O3 Thin Film by Sol–Gel Process," *Coatings 2021, Vol. 11, Page 1220*, vol. 11, no. 10, p. 1220, Oct. 2021, doi: 10.3390/COATINGS11101220.

[13] J. Jesenovec, M. H. Weber, C. Pansegrau, M. D. McCluskey, K. G. Lynn, and J. S. McCloy, "Gallium vacancy formation in oxygen annealed β-Ga2O3," *J. Appl. Phys.*, vol. 129, no. 24, Jun. 2021, doi: 10.1063/5.0053325.

[14] S. Zhang *et al.*, "Oxygen vacancies modulating performance for Ga2O3 solar-blind photodetectors via low-cost mist chemical vapor deposition," *Mater. Today Commun.*, vol. 39, p. 108717, Jun. 2024, doi: 10.1016/J.MTCOMM.2024.108717.

[15] P. Mandal, A. Mondal, A. Pandey, S. R. Meitei, and A. Bag, "Investigating role of annealing in shaping morphological,

structural, tribological, and optical characteristics of gallium oxide (Ga2O3): Insights from DFT analysis," *J. Alloys Compd.*, vol. 1011, p. 178367, Jan. 2025, doi: 10.1016/J.JALLCOM.2024.178367.
[16] Y. Yuan *et al.*, "Toward emerging gallium oxide semiconductors: A roadmap," *Fundam. Res.*, vol. 1, no. 6, pp. 697–716, Nov. 2021, doi: 10.1016/J.FMRE.2021.11.002.
[17] S. Wu, Z. Liu, H. Yang, and Y. Wang, "Effects of Annealing on Surface Residual Impurities and Intrinsic Defects of β-Ga2O3," *Crystals*, vol. 13, no. 7, p. 1045, Jul. 2023, doi: 10.3390/CRYST13071045/S1.

Information about authors:
Ruslan Kalibek – Master Student, Research Assistant, Faculty of Engineering, Süleyman Demirel University, 1/1 Almatinskaya st., Almaty, Kazakhstan, rus.kalibek@bk.ru
Daria Sopyryaeva – MSc, Academic Associate, Institute of Physics, Technical University of Berlin, 17 Straße des, Berlin, Germany, dsopyryaeva@mail.ru

Author Contributions:
Ruslan Kalibek – concept, methodology, resources, data collection, visualization, interpretation, drafting, funding acquisition.
Daria Sopyryaeva – testing, modeling, analysis, editing.

Conflict of Interest: The authors declare no conflict of interest.

Use of Artificial Intelligence (AI): The authors declare that AI was not used.

Received: 04.04.2026
Revised: 10.06.2026
Accepted: 21.06.2026
Published: 30.06.2026